IJOER
RESEARCH JOURNAL

International Journal of Engineering Research & Science

ISSN
2395-6992

www.ijoer.com
www.adpublications.org

Preface

We would like to present, with great pleasure, the inaugural volume-5, Issue-7, July 2019, of a scholarly journal, *International Journal of Engineering Research & Science*. This journal is part of the AD Publications series *in the field of Engineering, Mathematics, Physics, Chemistry and science Research Development*, and is devoted to the gamut of Engineering and Science issues, from theoretical aspects to application-dependent studies and the validation of emerging technologies.

This journal was envisioned and founded to represent the growing needs of Engineering and Science as an emerging and increasingly vital field, now widely recognized as an integral part of scientific and technical investigations. Its mission is to become a voice of the Engineering and Science community, addressing researchers and practitioners in below areas

Chemical Engineering	
Biomolecular Engineering	Materials Engineering
Molecular Engineering	Process Engineering
Corrosion Engineering	
Civil Engineering	
Environmental Engineering	Geotechnical Engineering
Structural Engineering	Mining Engineering
Transport Engineering	Water resources Engineering
Electrical Engineering	
Power System Engineering	Optical Engineering
Mechanical Engineering	
Acoustical Engineering	Manufacturing Engineering
Optomechanical Engineering	Thermal Engineering
Power plant Engineering	Energy Engineering
Sports Engineering	Vehicle Engineering
Software Engineering	
Computer-aided Engineering	Cryptographic Engineering
Teletraffic Engineering	Web Engineering
System Engineering	
Mathematics	
Arithmetic	Algebra
Number theory	Field theory and polynomials
Analysis	Combinatorics
Geometry and topology	Topology
Probability and Statistics	Computational Science
Physical Science	Operational Research
Physics	
Nuclear and particle physics	Atomic, molecular, and optical physics
Condensed matter physics	Astrophysics
Applied Physics	Modern physics
Philosophy	Core theories

Chemistry	
Analytical chemistry	Biochemistry
Inorganic chemistry	Materials chemistry
Neurochemistry	Nuclear chemistry
Organic chemistry	Physical chemistry
Other Engineering Areas	
Aerospace Engineering	Agricultural Engineering
Applied Engineering	Biomedical Engineering
Biological Engineering	Building services Engineering
Energy Engineering	Railway Engineering
Industrial Engineering	Mechatronics Engineering
Management Engineering	Military Engineering
Petroleum Engineering	Nuclear Engineering
Textile Engineering	Nano Engineering
Algorithm and Computational Complexity	Artificial Intelligence
Electronics & Communication Engineering	Image Processing
Information Retrieval	Low Power VLSI Design
Neural Networks	Plastic Engineering

Each article in this issue provides an example of a concrete industrial application or a case study of the presented methodology to amplify the impact of the contribution. We are very thankful to everybody within that community who supported the idea of creating a new Research with IJOER. We are certain that this issue will be followed by many others, reporting new developments in the Engineering and Science field. This issue would not have been possible without the great support of the Reviewer, Editorial Board members and also with our Advisory Board Members, and we would like to express our sincere thanks to all of them. We would also like to express our gratitude to the editorial staff of AD Publications, who supported us at every stage of the project. It is our hope that this fine collection of articles will be a valuable resource for *IJOER* readers and will stimulate further research into the vibrant area of Engineering and Science Research.

Mukesh Arora

(Chief Editor)

Board Members

Dr. Aurora Angela Pisano

Ph.D. in Civil Engineering, Currently Serving as Associate Professor of Solid and Structural Mechanics (scientific discipline area nationally denoted as ICAR/08"–"Scienza delle Costruzioni"), University Mediterranea of Reggio Calabria, Italy.

Dr. Faizullah Mahar

Associate Professor in Department of Electrical Engineering, Balochistan University Engineering & Technology Khuzdar. He is PhD (Electronic Engineering) from IQRA University, Defense View,Karachi, Pakistan.

Dr. S. Kannadhasan

Ph.D (Smart Antennas), M.E (Communication Systems), M.B.A (Human Resources).

Dr. Christo Ananth

Ph.D. Co-operative Networks, M.E. Applied Electronics, B.E Electronics & Communication Engineering Working as Associate Professor, Lecturer and Faculty Advisor/ Department of Electronics & Communication Engineering in Francis Xavier Engineering College, Tirunelveli.

Dr. S.R.Boselin Prabhu

Ph.D, Wireless Sensor Networks, M.E. Network Engineering, Excellent Professional Achievement Award Winner from Society of Professional Engineers Biography Included in Marquis Who's Who in the World (Academic Year 2015 and 2016). Currently Serving as Assistant Professor in the department of ECE in SVS College of Engineering, Coimbatore.

Dr. Maheshwar Shrestha

Postdoctoral Research Fellow in DEPT. OF ELE ENGG & COMP SCI, SDSU, Brookings, SD
Ph.D, M.Sc. in Electrical Engineering from SOUTH DAKOTA STATE UNIVERSITY, Brookings, SD.

Zairi Ismael Rizman

Senior Lecturer, Faculty of Electrical Engineering, Universiti Teknologi MARA (UiTM) (Terengganu) Malaysia Master (Science) in Microelectronics (2005), Universiti Kebangsaan Malaysia (UKM), Malaysia. Bachelor (Hons.) and Diploma in Electrical Engineering (Communication) (2002), UiTM Shah Alam, Malaysia

Dr. D. Amaranatha Reddy

Ph.D.(Postdocteral Fellow,Pusan National University, South Korea), M.Sc., B.Sc. : Physics.

Dr. Dibya Prakash Rai

Post Doctoral Fellow (PDF), M.Sc.,B.Sc., Working as Assistant Professor in Department of Physics in Pachhuncga University College, Mizoram, India.

Dr. Pankaj Kumar Pal

Ph.D R/S, ECE Deptt., IIT-Roorkee.

Dr. P. Thangam

BE(Computer Hardware & Software), ME(CSE), PhD in Information & Communication Engineering, currently serving as Associate Professor in the Department of Computer Science and Engineering of Coimbatore Institute of Engineering and Technology.

Dr. Pradeep K. Sharma

PhD., M.Phil, M.Sc, B.Sc, in Physics, MBA in System Management, Presently working as Provost and Associate Professor & Head of Department for Physics in University of Engineering & Management, Jaipur.

Dr. R. Devi Priya

Ph.D (CSE),Anna University Chennai in 2013, M.E, B.E (CSE) from Kongu Engineering College, currently working in the Department of Computer Science and Engineering in Kongu Engineering College, Tamil Nadu, India.

Dr. Sandeep

Post-doctoral fellow, Principal Investigator, Young Scientist Scheme Project (DST-SERB), Department of Physics, Mizoram University, Aizawl Mizoram, India- 796001.

Mr. Abilash

MTech in VLSI, BTech in Electronics & Telecommunication engineering through A.M.I.E.T.E from Central Electronics Engineering Research Institute (C.E.E.R.I) Pilani, Industrial Electronics from ATI-EPI Hyderabad, IEEE course in Mechatronics, CSHAM from Birla Institute Of Professional Studies.

Mr. Varun Shukla

M.Tech in ECE from RGPV (Awarded with silver Medal By President of India), Assistant Professor, Dept. of ECE, PSIT, Kanpur.

Mr. Shrikant Harle

Presently working as a Assistant Professor in Civil Engineering field of Prof. Ram Meghe College of Engineering and Management, Amravati. He was Senior Design Engineer (Larsen & Toubro Limited, India).

Table of Contents

Smart and Economical Scheme for Electrical Power Generation

Ahmed A. Hafez[1], Abed Alrzaq S. Alshqirate[2*], Ahmed Y. Hatata[3], Khaled S. Alharbi[4], Mohammed Alotabi[5], Abdurhman S. Alotabi[6], Khalf M. Alotabi[7], Mohammed A. Almutari[8], Munif S. Almutari[9]

[1,3-9]Elect. Eng. Dept., College of Eng., Shaqra University, Kingdom of Saudi Arabia
[*2]Mech. Eng. Dept., College of Eng., Shaqra University, Kingdom of Saudi Arabia
[*2]Al-Balqa Applied University, Al-Salt, 19117, Jordan

Abstract— *This article advises a simple and innovative scheme for generating electricity from human activities. A simple and robust approach is proposed for converting human walking into valuable electricity source. The proposed scheme could be sufficient for powering small portable devices and providing independent power supply. Matlab and Simulink dynamic platform are used for stimulating the systems under concern. The prototype results validate the simulation results. The proposed scheme proofed to be valuable, economical and reliable power supply*.

Keywords— Pressure, Energy converter, Electricity, Boost converter, Portable.

I. INTRODUCTION

The electricity demand is increasing very rapidly, which requires building more fossil fuel power plants to supply such load. However, fossil fuel plants suffer from numerous drawbacks. They are main source of pollution. Tons of greenhouse gases as CO_2 are released, which causes global warming, desertion and flooding. Moreover, traditional power plants have high running and maintenance costs [1,2]. Furthermore, the limited reserve of fossil fuels motives the search for alternative energy sources.

The researchers are searching for eco-friendly and sustainable power source. Solar and wind energies are investigated. However, the stochastic nature and weather dependency reduce the advantages of these sources. Moreover, wind energy involves complex and costly system for generating electricity [3].

This article proposes a new scheme for generating electricity from human footsteps. A simple and efficient mechanical device is proposed that converts the footstep pressure into energy. An efficient and simple electronic circuit is advised for harvesting the generated power. A prototype was built to test the functionality of the proposed scheme. Matlab and its dynamic platform Simulink are used for stimulating the proposed systems. The practical and simulation results are introduced to validate the proposed generation method.

II. SYSTEM LAYOUT

The proposed system consists of energy converter, generator, diode rectifier, DC boost converter, battery and load as shown in Figure 1.

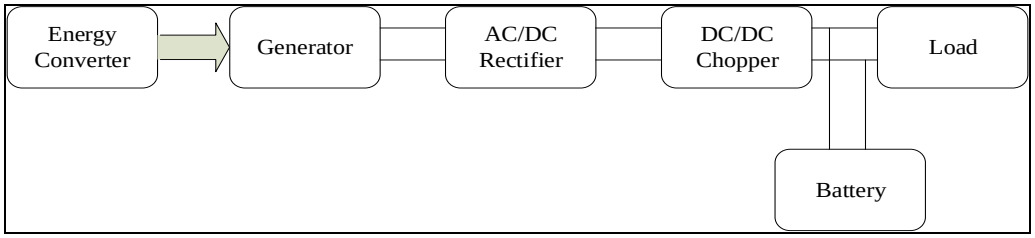

FIGURE 1. Block diagram of the proposed system

The battery is added to the proposed system to store the generated electricity. The power could be supplied to the load directly or stored in the battery depending on the load specification. Then, the battery feeds the load.

2.1. Energy converter

A mechanical device is used to converter the step into a mechanical energy. Figure 2 shows the energy converter. This device is designed to be simple and integrated easily on the structures involving human activities.

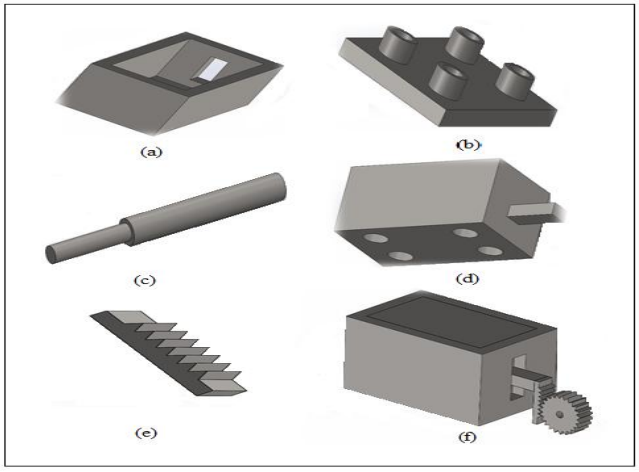

FIGURE 2. The mechanical parts of the designed prime mover

The main parts of the prime mover shown in Figure 2 are:

1. Part (a) is iron box with some holes and installation places inside it.
2. Part (b) is placed in part (a), it contains springs inside each slot to be controlled by the coming down and step surface height.
3. Part (c) is a rotating shaft, where the generator rotor is mounted.
4. Part (d) is installed above part (b) and it is free to move up and down.
5. Part (e) is installed with part (d) and it free to move up and down within part (d).
6. Part (f) is the container, where all the parts are installed.

The pressure on the upper part of the mechanical converter would result in freely up/down movement. The force would be produced due to the pressure, as given by,

$$F = P \times A \tag{1}$$

Where P is the pressure (N/m^2), A(m^2)

This force would produce motion; the linear velocity is related to the force by,

$$v = \frac{1}{m}\int F dt \tag{2}$$

Where, m is the mass of pressed, the output energy is given by

$$w = \frac{F}{m}\int F dt \tag{3}$$

2.2. DC Generator

A Permanent Magnet PMDC generator is used for converting mechanical energy in to electrical energy. This DC generator has simple structure due to existence of permanent field excitation [4]. The equivalent circuit that depicts the operation principle of the DC generator is shown in Figure 3.

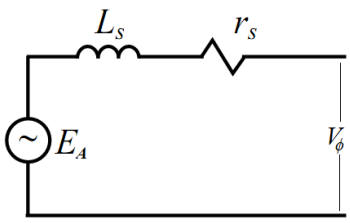

FIGURE 3. Equivalent circuit of PMDC

The operation of the PMDC for generation could be depicted by a 1st order differential and swing equations as given by [4],

$$\frac{di_a}{dt} = \frac{1}{L_a}\left(\omega_r \varphi - V_a - r_a i_a\right) \tag{4}$$

$$T_e = k_T \varphi i_a \tag{5}$$

$$T_m - T_e = J\frac{d\omega_r}{d} \tag{6}$$

Where, i_a, L_a, r_a and V_a are armature current, self-inductance, resistance and voltage respectively. ω_r , φ , T_e, T_m are angular velocity, flux, generator torque and prime mover torque respectively.

2.3. Diode rectifier

Mechanical mover , Figure 1, moves up and down; therefore the direction of rotation of the DC generator reverses with varaible amplitude. A full bridge diode recrtifier is applied to rectify the generator output voltage. Very low voltage drop diodes are chosen for implementing the diode rectifier [5-8].

2.4. DC Boost Converter

A boost converter is used to ensure constant output voltage and produce acceptable level for batteries. The boost circuit has two statuses: on and off-states. The dynamic performance model of the boost converter could be depicted from these states topology. Averaging over a switching cycle, the dynamic performance of the boost chopper could be given by [9-13],

$$L\frac{di_L}{dt} = V_{dc} - V_o(1-D) \tag{7}$$

$$C_o\frac{dV_o}{dt} = -\frac{V_o}{R_L} + i_L(1-D) \tag{8}$$

A Proportional Integral (PI) controller is used to ensure constant output voltage, V_o. The PI compensator is tuned via Nichols-Ziegler reaction time empirical method [14]. The parameters of the PI controller are given in Table1

TABLE 1
PARAMETERS OF PI CONTROLLER

Proportional gain k_p	0.1
Integral gain k_i	2

III. RESULTS AND DISCUSSIONS

Matlab dynamic platform, Simulink, is used for stimulating the system under consideration. Figures 4-6 shows the input force of the footstep, generated voltage, the diode dc voltage and the boost converter output voltage.

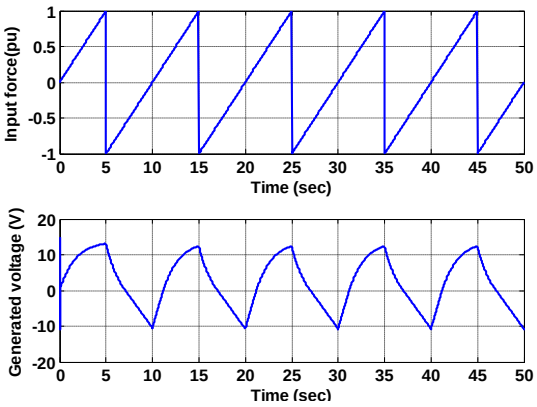

FIGURE 4. Input force (pu) top graph, generator output voltage (V) bottom graph

Figure 4 shows waveform of the force, which is exerted on the energy converter. This force is due to the pressed footstep and the spring in the energy converter itself. The generated voltage has bidirectional nature.

Figure 5 shows that the H-bridge diode rectifier converts the bidirectional generated voltage into useable DC voltage. However, the voltage level is still below the required. Therefore, a boost converter is employed for boosting the DC voltage into acceptable level

Figure 6 shows that boost converter increases the H-bridge rectifier voltage from 2.8V to around 9.8V. The boost operates with around 71% duty cycle, where the input voltage is boosted around 350%.

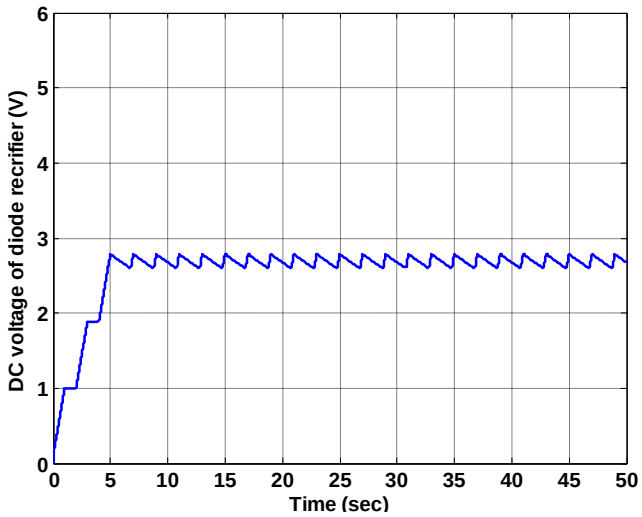

FIGURE 5: DC voltage of the diode rectifier

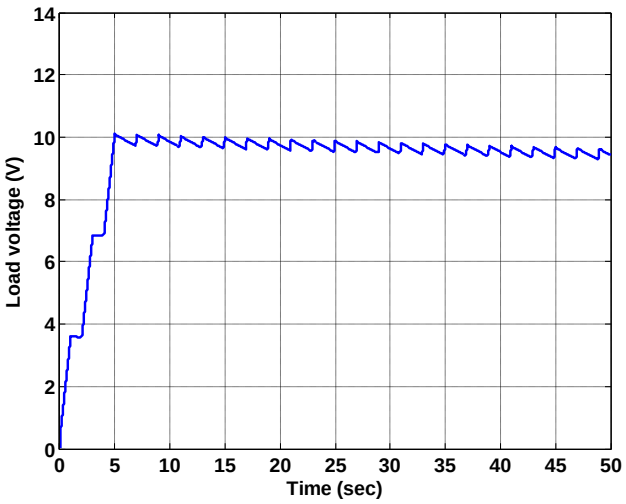

FIGURE 6: the boost converter output voltage

IV. PROTOTYPE OF THE PROPOSED GENERATION SYSTEM

A prototype was built as shown in Figure 7.

The output voltage of generator, diode rectifier and the boost converters are shown in Figures 8, 9 and 10 respectively.

Figure 8 shows that generated output voltage from the proto-type is bidirectional, this complies with figure 4. However, the difference due to the assumption and ideal components used in the simulation.

Figure 9 shows that the H-bridge diode rectifier converts the bidirectional voltage into DC voltage. Figure 9 shows that the DC voltage is almost ripple free, which is attributed to the capacitor size.

Figure 10 shows that the boost converter boosts the output voltage of the rectifier to the desired level.

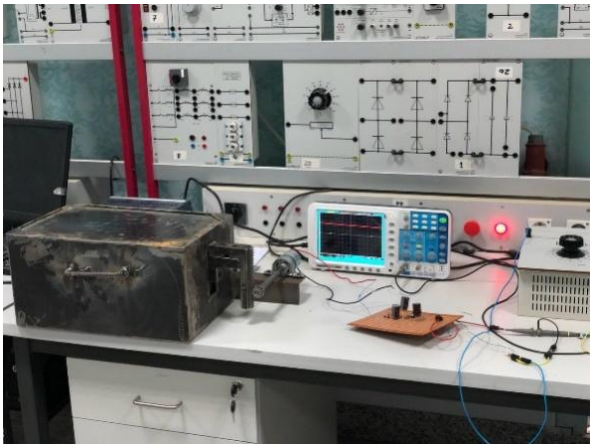

FIGURE 7. A prototype of the footstep electrical power generation

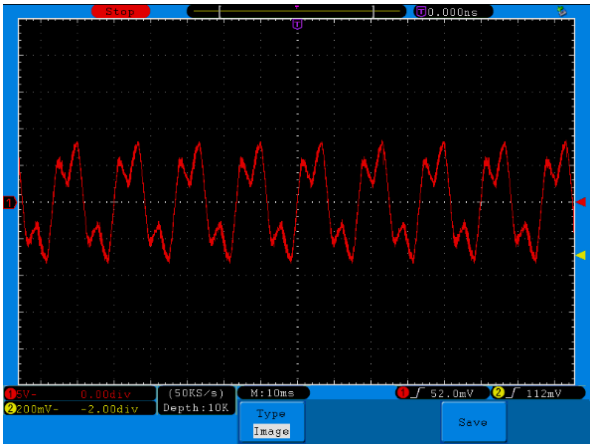

FIGURE 8. Generator output voltage

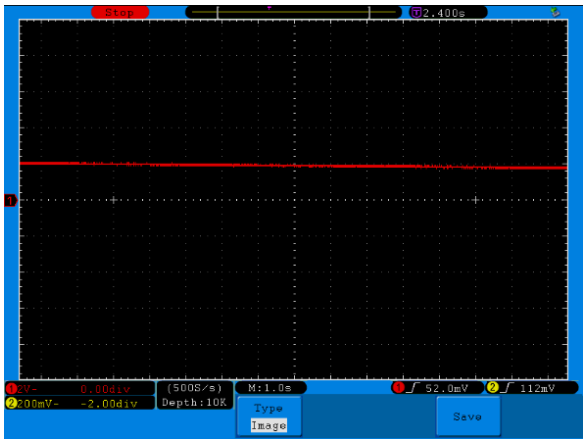

FIGURE 9. Diode rectifier output voltage

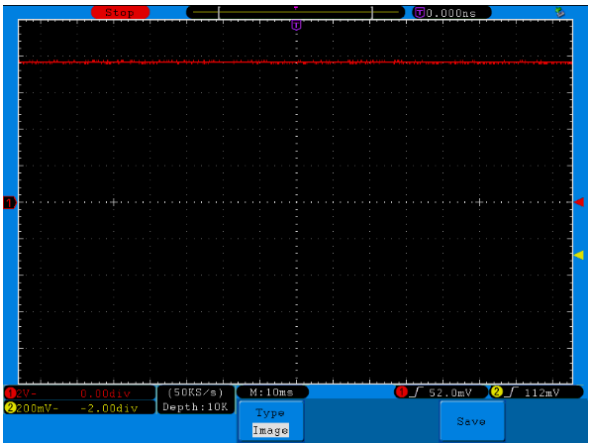

FIGURE 10: Boost converter output voltage

The feasibility of the proposed scheme proved by Figures 8-10, that itt could be valuable source for lighting

1- Figure 8 shows that the generated voltage is bidirectional, which is attributed to the mechanism of prime mover movement.

2- Figure 9 shows that the rectifier converter the bidirectional form of the generator output voltage into DC voltage. The DC voltage is shown to have small ripple content; this is due to the application of large DC capacitor.

3- Figure 10 shows that the boost converter boosts the output voltage of the rectifier to the desired level.

These figures confirm the functionality of the proposed idea. It is worth to mention that the output power is likely not enough to supply high power load.

V. CONCLUSION

Innovative scheme for generating electricity from main human activity, which is walking advised in this article. Simple and elaborate design for the energy converter convert human footstep into mechanical energy designed and implemented. This energy converter could be integrated with structures as stairs. PMDC generator, diode rectifier and boost converter are attached to the prime mover. The rectifier is used to rectify the output voltage as it fluctuates due to the mechanism of shaft rotation. The produced power is sufficient for charging portable devices. The practical setup validates simulation results, which proves the feasibility of this approach.

It is worth to mention that this scheme is notable for producing a power level required for a reasonable load. Moreover, this arrangement requires high flow of the people to generate electricity.

REFERENCES

[1] F. Shahnia, "Stability of a sustainable remote area microgrid," *2016 IEEE Region 10 Conference (TENCON)*, Singapore, 2016, pp. 1220-1223.

[2] A. K. Nayak, P. Sarangi, R. Santra and A. K. Kotini, "Economic generation mix for commercial building," *2014 14th International Conference on Environment and Electrical Engineering*, Krakow, 2014, pp. 249-253.

[3] N. Nikmehr and S. Najafi Ravadanegh, "A heuristic load flow algorithm for active distribution grids," *2013 Smart Grid Conference (SGC)*, Tehran, 2013, pp. 31-35.

[4] O.Wasynczuk, P. C. Krause, Scott D. Sudhoff, and Steven Pekarek" Analysis of Electric Machinery and drive systems" 3rd editon, IEEE press, Wiley, 2002.

[5] H. Shin and J. I. Ha, "Active DC-link circuit for single-phase diode rectifier system with small capacitance," *2014 International Power Electronics and Application Conference and Exposition*, Shanghai, 2014, pp. 875-880.

[6] Y. Son and J. I. Ha, "Efficiency improvement in motor drive system with single phase diode rectifier and small DC-link capacitor," *2014 IEEE Energy Conversion Congress and Exposition (ECCE)*, Pittsburgh, PA, 2014, pp. 3171-3178.

[7] T. Sakkos and V. Sarv, "A new high power factor single-phase diode rectifier with optimum ripple-power conversion," *2006 International Biennial Baltic Electronics Conference*, Tallinn, 2006, pp. 1-4.

[8] Y. Ji and F. Wang, "Single-phase diode rectifier with novel passive filter," in *IEE Proceedings - Circuits, Devices and Systems*, vol. 145, no. 4, pp. 254-259, Aug 1998.

[9] Mattos, A. M. S. S. Andrade, G. V. Hollweg, J. Renes Pinheiro and M. Lucio da Silva Martins, "A REVIEW OF BOOST CONVERTER ANALYSIS AND DESIGN IN AEROSPACE APPLICATIONS," in *IEEE Latin America Transactions*, vol. 16, no. 2, pp. 305-313, Feb. 2018.

[10] J. Arrozy, J. H. F. Rajagukguk, A. Rizqiawan and P. A. Dahono, "Performance evaluation of large ratio dc-dc boost converter," *2017 4th International Conference on Electric Vehicular Technology (ICEVT)*, Bali, Indonesia, 2017, pp. 55-60.

[11] M. Veerachary, "Third-order boost converter," in *IET Power Electronics*, vol. 11, no. 3, pp. 566-575, 3 20 2018.

[12] W. Jiang, S. H. Chincholkar and C. Y. Chan, "Comparative study of adaptive current-mode controllers for a hybrid-type high-order boost converter," in *IET Power Electronics*, vol. 11, no. 3, pp. 524-530, 3 20 2018.

[13] H. Han, R. Tan, J. Yang, H. Wang, S. Ning and M. Shen, "A novel efficient tri-state boost converter," *2017 IEEE Electrical Power and Energy Conference (EPEC)*, Saskatoon, SK, 2017, pp. 1-6.

[14] R. S. Burns" Advanced Control Engineering" 1st edition, Butterworth-Heinemann, 2001.

Manual Correction of Myopia, Hypermetropia, Astigmatism, Presbyopia & Keratoconus.

[1]Prof. Bijay Kumar Parida, MS, FRCS
[2]Ms. Anannya Anupurva

[1]Muthusamy Virtual University of Post Graduate Ophthalmology
[2]MVJ Medical College.

Abstract— *A new method has been designed to correct myopia, hypermetropia, astigmatism and presbyopia of very high power. If 1mm of cornea is tucked, then it corrects* ***3.174 D*** *& If 1mm of horizontal diameter of cornea is reduced, then it corrects* ***+4.1D.*** *This procedure is reliable, safe, cheapest and simplest. Because of the use of simple procedure to split the cornea, adjustable nonabsorbable sutures, correction of very high myopia and hypermetropia along with astigmatism and presbyopia, the procedure is expected to be accepted.*

Keywords— Arc of cornea, chord, angle of arc, myopia, hypermetropia, astigmatism, formula.

I. INTRODUCTION

LASIK (laser-assisted in situ keratomileusis) is a type of refractive surgery for the correction of myopia, hypermetropia and astigmatism. LASIK is most similar to another surgical corrective procedure, photorefractive keratectomy (PRK), and LASEK. All represent advances over radial keratectomy in the surgical treatment of refractive errors of vision. For patients with moderate to high myopia or thin corneas which cannot be treated with LASIK and PRK, the phakic intraocular lens is an alternative.[1,2]

Some people with poor outcomes from LASIK surgical procedures report a significantly reduced quality of life because of vision problems or physical pain associated with surgery. However, 30% of post-LASIK referrals to tertiary ophthalmology care centers have been shown to be due to chronic dry eye.[3,4].

A type of LASIK, known as presbyLASIK, may be used in presbyopia.[5]

Flap complications,[6,7,8,9] slipped flap and flap interface particles are other complications.

Together with his colleagues, Charles Munnerlyn founded VISX USA inc.

SMILE is an acronym that stands for "Small Incision Lenticule Extraction" and is the latest advancement in laser vision correction. During a SMILE procedure, the femtosecond laser is used to cut a small corneal lenticule (precise lens shaped disc within cornea) and then it is removed via a small keyhole incision. The biggest difference and advancement between the two is the fact that SMILE laser eye surgery is a flapless procedure.

II. PRINCIPLE

If the curvature of cornea is responsible for myopia or hypermetropia, it can either be flattened or steepened to change the power of cornea. For example, if the cornea is made flatter, then the myopia is reduced. Whereas, if the cornea is made steeper, then the power of the cornea is increased, refractive index of the cornea and other factors responsible for ocular refractive power remaining unchanged. Assuming the refractive power of anterior surface of cornea is +49D, after deducting -6D power of posterior surface of cornea, the net power of cornea is +43D.

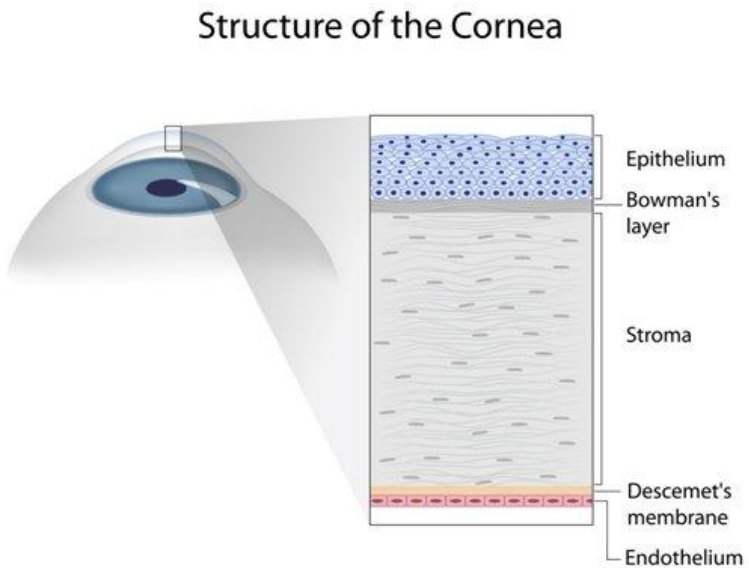

FIGURE 1

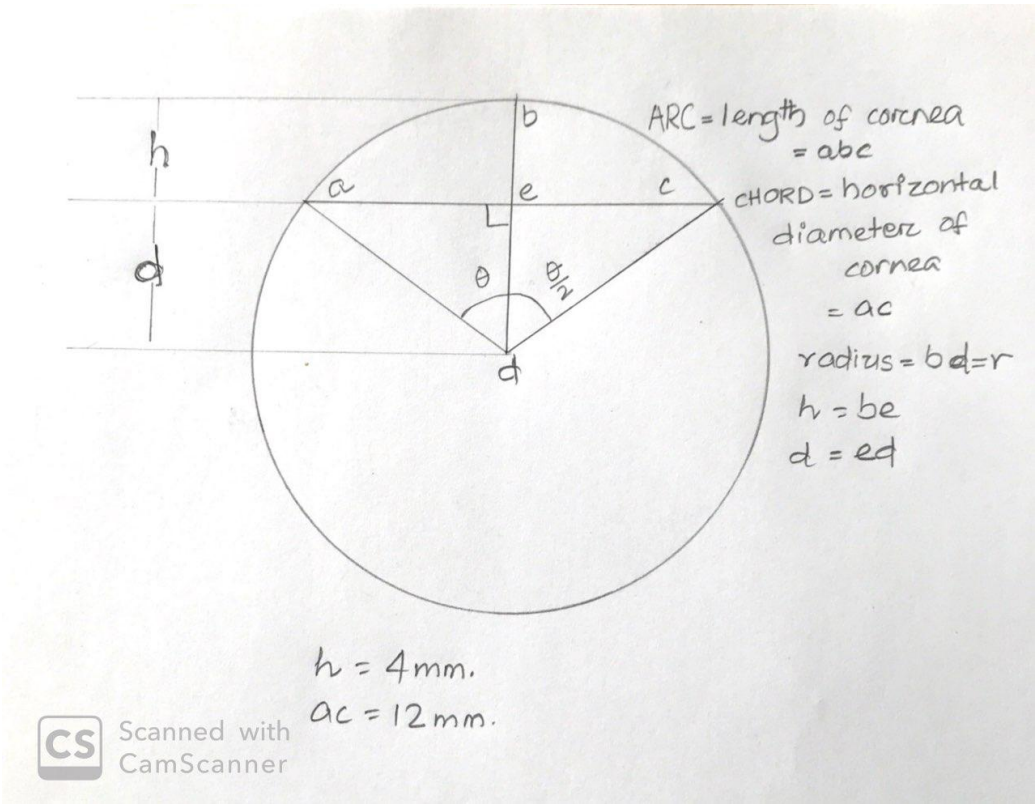

FIGURE 2

c=horizontal diameter of cornea=12mm=chord of this circle,

h=4mm, the distance between endothelium & iris plane.

radius=[h÷2]+[cxc÷8h]

In this case h=4mm, c=12mm

So 4/2 + 12x12/8x4

=13/2=6.5mm

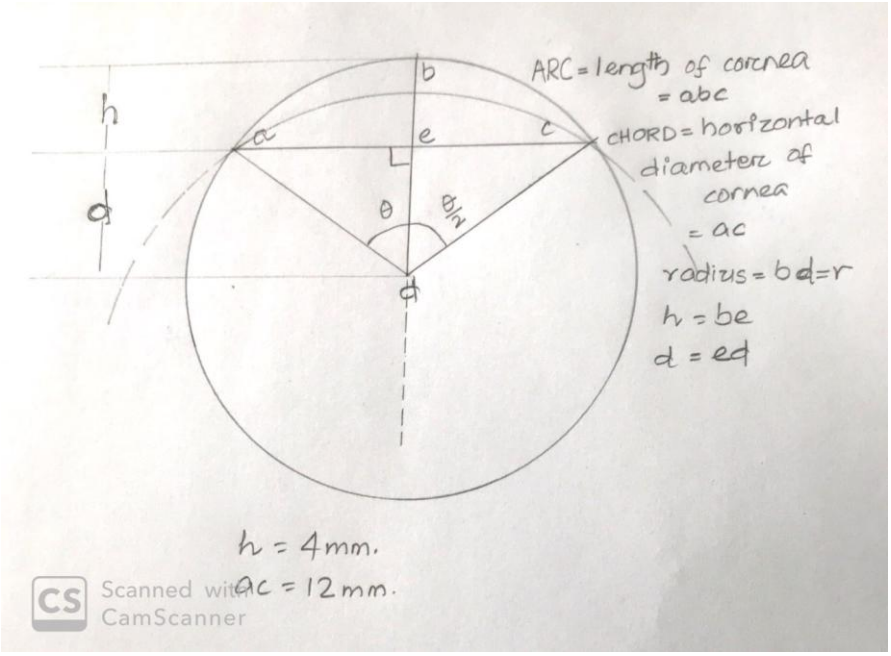

FIGURE 3

So d=6.5-4=2.5mm

sin θ=c/2 ÷r=12/2 ÷13/2=12/13=68°

Total angle of arc is 136°

II. Arc length= (angle of arc ÷360°) x 2πr

=(136÷360)÷(2x22/7x13/2)=15.4349215mm=**length of cornea**

III.15.4349215 OR 15.44 mm at arc angle at 136°, has power of +49D.As inner cornea has -6D power, the net power of cornea is +43D. So, keeping other factors constant, reduction of 1mm of cornea in length, shall reduce the power by 3.17357513 D (49÷15.4349215).This is approximately **3.174 D**.

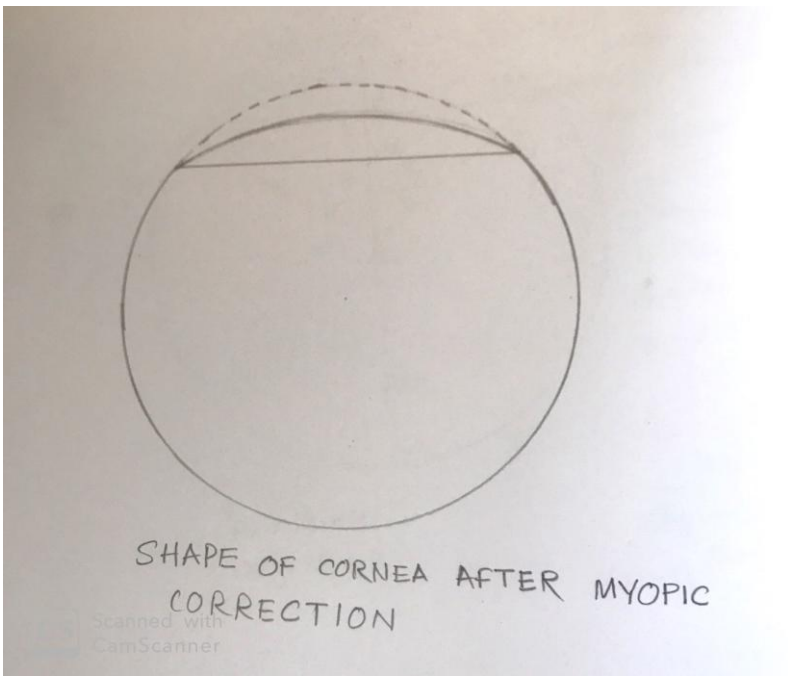

FIGURE 4

If 1mm of cornea is tucked on either sides that will flatten the cornea and correct 2 x 3.174 =6.348D of myopia. If 0.5 mm of cornea is tucked, then correction of 3.174 ÷ 2=1.587D of myopia.

2mm of cornea on either side (4mm) is tucked; 11 mm of cornea is left. If 3mm on either sides of cornea is tucked(=6mm in total), then 9mm is left to be flattened. If 4 mm on either sides is tucked (8mm), then 7 mm is left. If 5mm on either sides is tucked (10mm), then 5mm of clear cornea is left. Central cornea of 4 mm is essential to be clear.

Thus (10 x 3.174=) **-31.74D can be corrected, which is equal to (31.74-6=) 25.74D.**

FORMULA; D2=[(Pc÷Lc)x(Lt)]-6

Pc=power of anterior surface of cornea.

Lc =length of cornea=(θ÷360°)x2πr

Lt=length of cornea tucked.

Sin θ = perpendicular÷hypotenuse=p/h

Example: myopia of **-20 D spherical & -6 cylindrical error at 90 °.**

***7.179000858=7.18mm of cornea** has to be replicated. On either sides 3.59mm to be tucked.

*to correct -6 cylindrical, 2.15370257 mm (=2.154mm) has to be plicated.

So 1.07685129 (= 1.1mm) on either sides of cornea at 180° to be tucked more at 180°.So at 180°,3.6+1.1=4.7mm has to be tucked.

Except 1mm of peripheral cornea at periphery and 4 mm at center, rest of the cornea is available for the procedure.

VII. Similarly, 12mm of horizontal diameter of cornea, other conditions remaining constant is associated with +49D. **So 1mm of horizontal diameter is associated with +4.08333333(=+4.1D)**

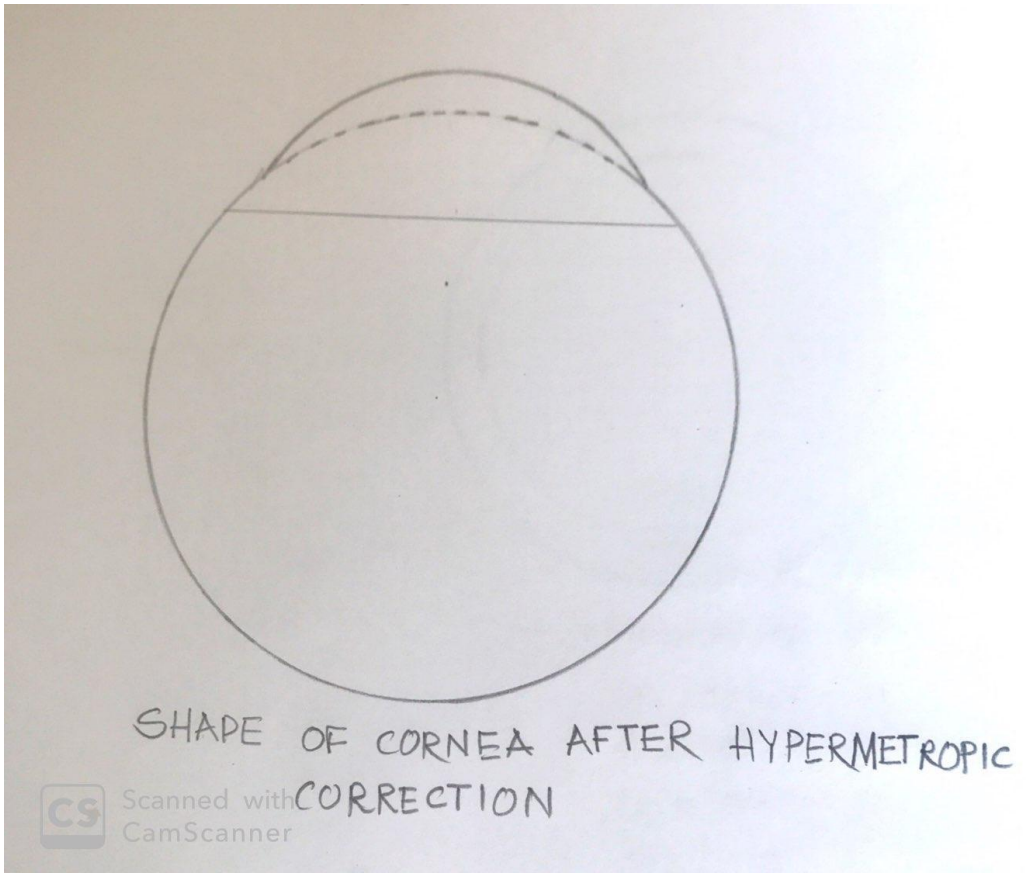

FIGURE 5

Cornea covering 4mm of pupil shall be left free 8 mm of horizontal diameter of cornea can be tucked i.e. 4mm on either sides.4mm + 4mm=8 x 4.1= 32.4 D of hypermetropia can be corrected. **So net correction of hypermetropia possible is 32.4-6=26.4 D.**

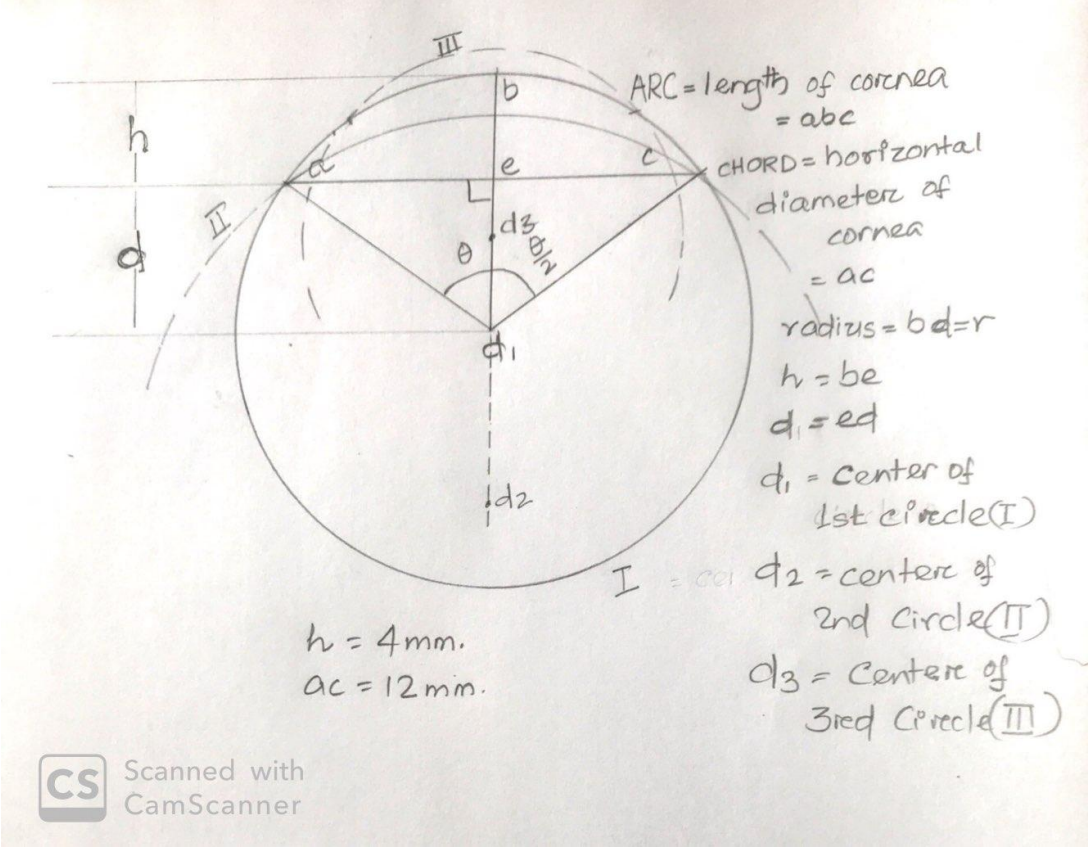

FIGURE 6

Site of application of suture is equal to the cornea to be squeezed. In this case 3.35mm above limbus on either sides.

Formula: D2=Pc÷Hc

Pc=Power of anterior surface of cornea (D1).

Hc=Horizontal diameter of cornea

Example: + 18 spherical +6 cylindrical power at 180°.Transposing it ,it is clear that +24 spherical and -6 cylindrical power at 90° is required to be changed.6.7mm of horizontal diameter out of 12mm (8mm maximum available) has to be squeezed by purse string suture. On all sides, 3.35 mm is squeezed and on top of it, 1.1mm of cornea has to be tucked on either side at 90°.

PRESBYOPIC CORRECTION: Maximum +3D is planned to be corrected. But correction is dependent on age of the patient. Lower 40% of cornea is to be made hypermetropic. The sutures are type of purse string, which is tied at 0.75 mm above limbus. But squeezed to reduce by 25 mm only. This is measured by a caliper to measure curved surface. If fully tightened, then it shall measure 11.25mm.This will correct presbyopia of 3d.If 1D correction is required, then horizontal diameter of cornea must be11.75mm .

III. MATERIAL & METHOD

3.1 Manual Method

1. scleral tunnel blade, having convex angle.

2. Length of blade 10mm & width 4mm.

3. Spatula 10mm x 4mm

4. 2 types of caliper specially designed of measurement of curvature.

5. Fine tip marker pen

6. Gentian violet

7. 8-0 prolene sutures

8. Fine tooth forceps

9. Needle holder

10. Tie forceps

3.2 Procedure:

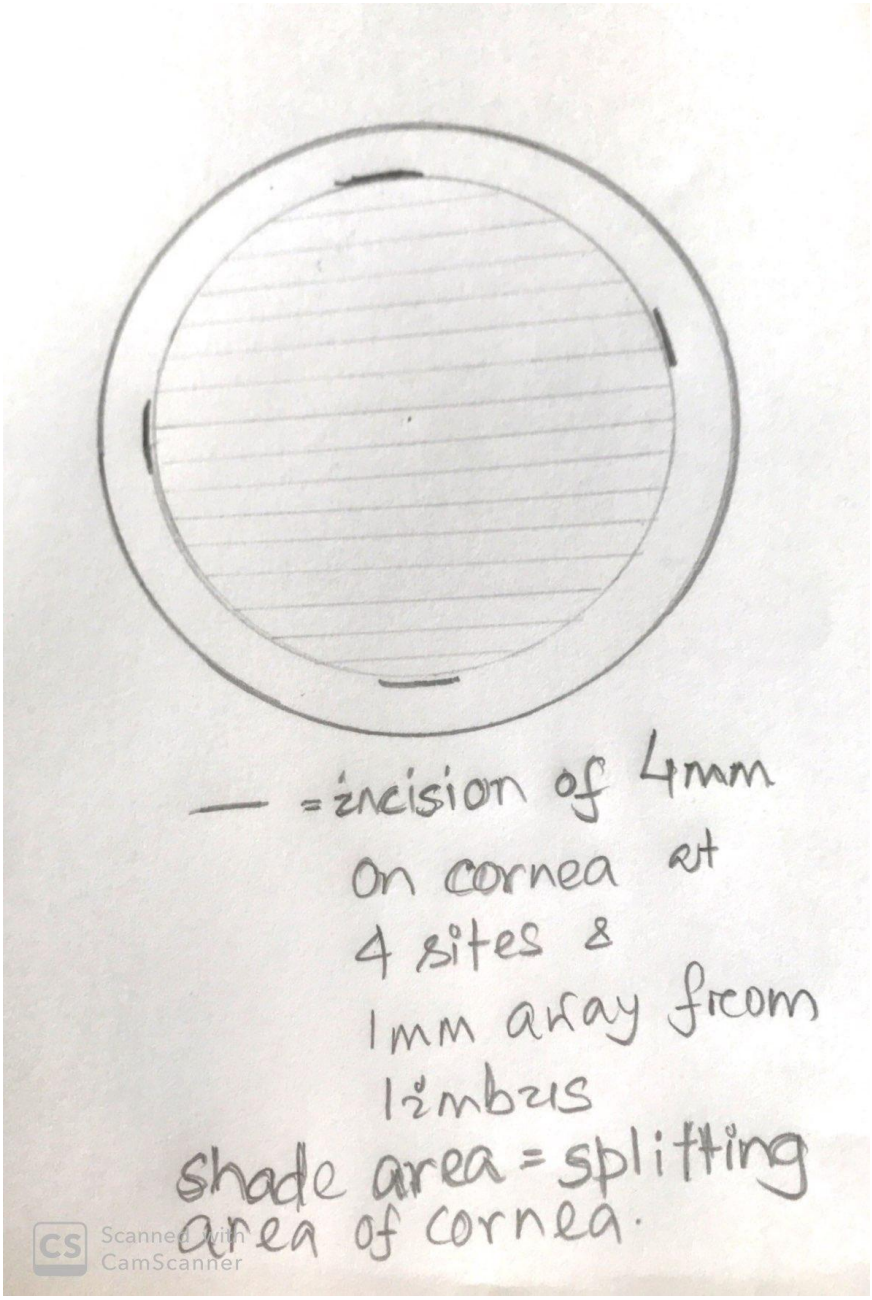

FIGURE 7

Myopia; firstly, 1mm away from limbus ,a 4mm wide incisions are made to a depth of 0.15mm.On this plane, a scleral tunnel blade can split cornea stroma into 2 parts,and the splitting is extended upto centre of cornea. Similarly, the cornea is

split from diagonally opposite site(if 1st one at 0° axis, then the 2nd one on 180° axis.) similarly, incision and splitting is done form 90° and 270°.The splitting of the cornea is completed in 360° to free the epithelial layer from stroma.

Method to plicate part of cornea is by running a sure through cornea at 3/4th depth & come out at desired end of the length. Then similarly run it from opposite side and exit near the point of entry, preferably 4 mm wide, to take adequate bite and tuck it as well as prevent cheese cutting.

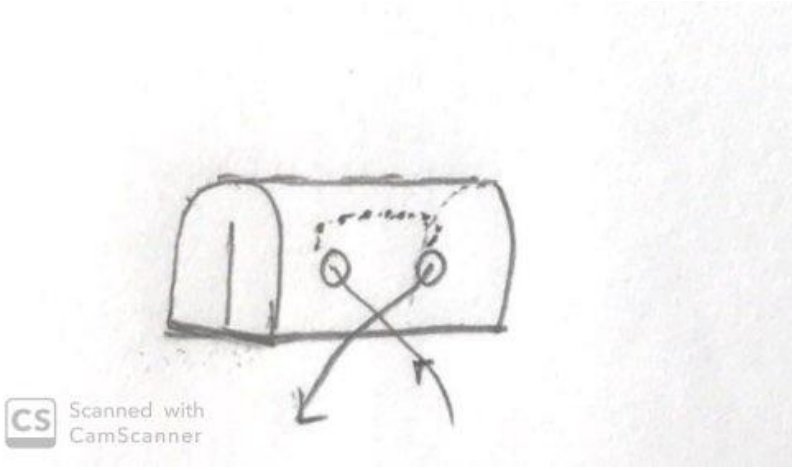

FIGURE 8

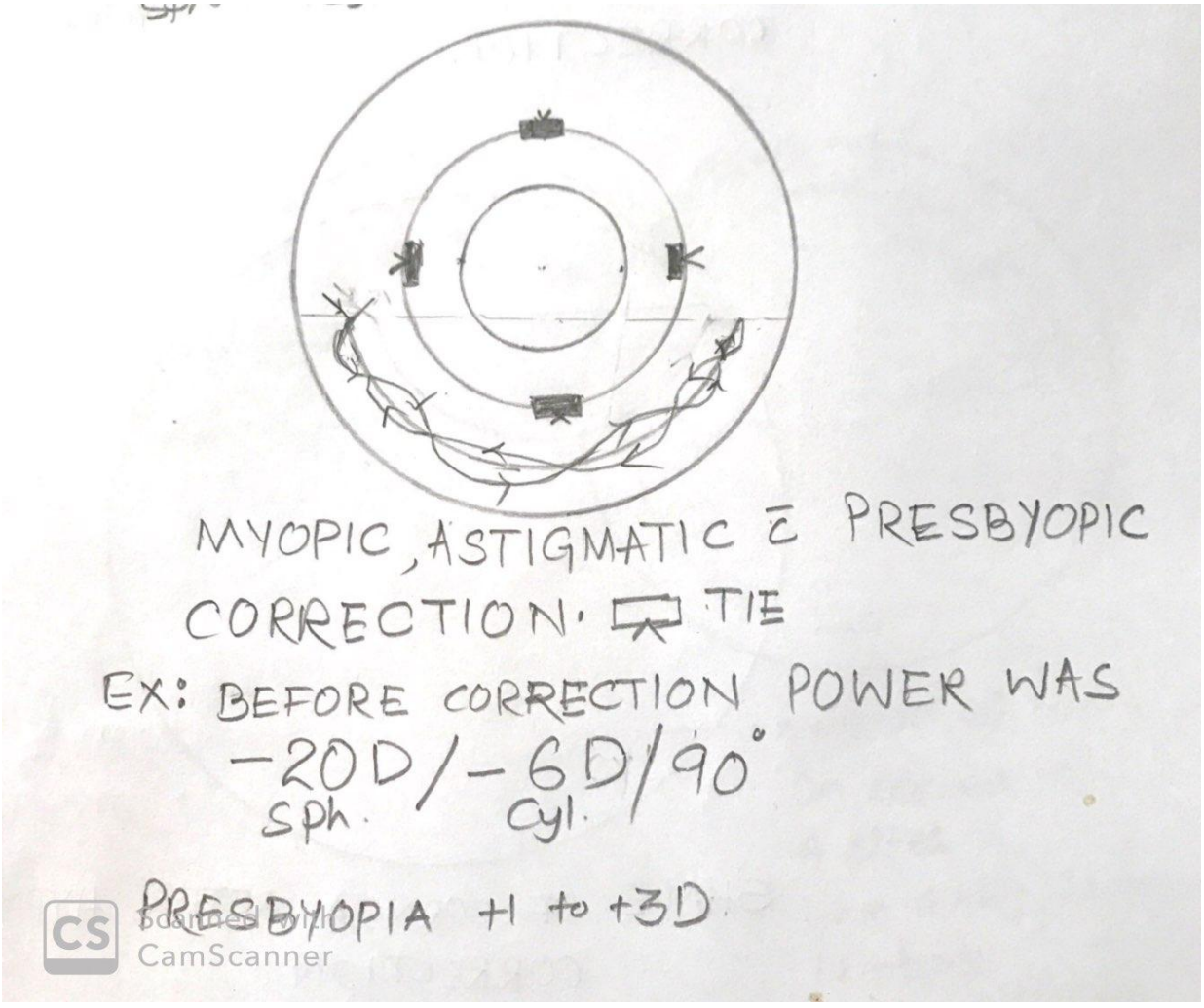

FIGURE 9

Hypermetropia:

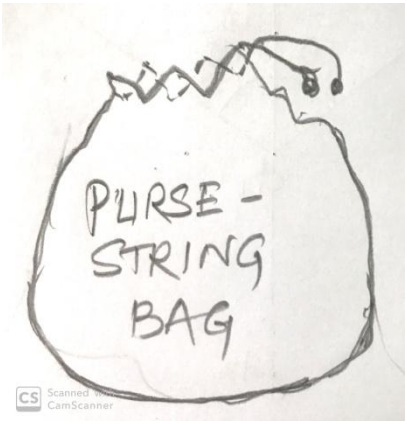

FIGURE 10

Incision on cornea is made on the site depending on the hypermetropia to be corrected. If 1mm of horizontal diameter of cornea to be reduced, then incision to be made 1mm away from limbus.

The cornea split as mentioned in correction of myopia.

In this case a prolene suture runs in purse-string fashion, so that when it is pulled, it narrows the horizontal diameter of the cornea in order to correct hypermetropia more than required, so that myopic shift can be corrected.

Adjustable sutures can be used to correct the errors according to portable keratometre measurement or verifying in operation theater by automatic keratometre or as found on 1st post op day.

Subsequently, astigmatism can be corrected above the purse string suture.

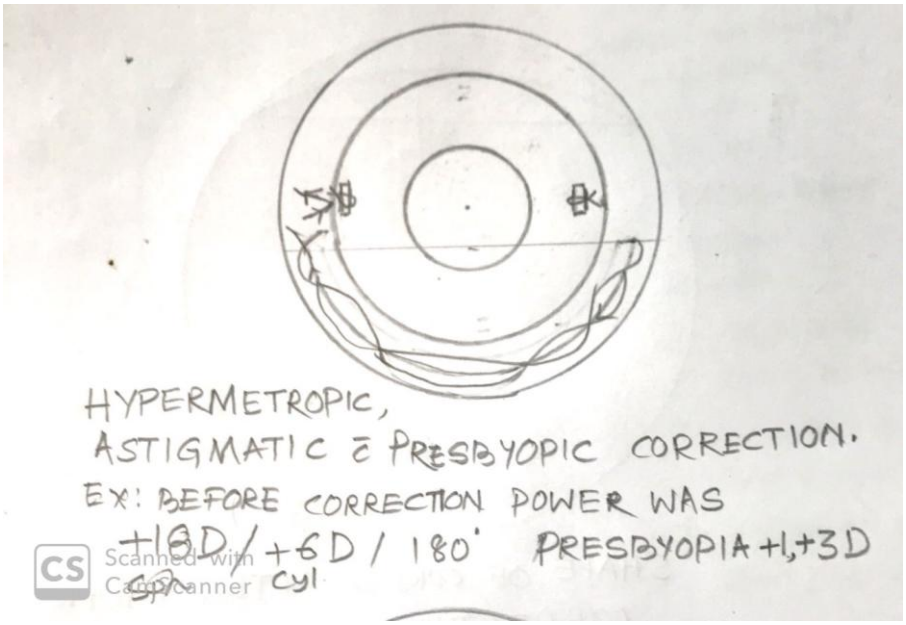

FIGURE 11

Presbyopia: (CORRECTION IS SHOWN IN ABOVE TWO DIAGRAMS ALONG WITH OTHER CORRECTIONS)By reducing the horizontal diameter of cornea to increase the power of the eye at lower 40% (2/5th) of cornea. A suture runs as in hypermeropic correction but only lower 40%. The running purse string suture passes through cornea at 0.75 mm from limbus as it ads +3D power to cornea at lower half only .This suture can be added to either myopic or hypermetropic or astigmatism corrections.

IV. ADVANTAGES

1. It does not require femtosecond or excimer laser which is exuberantly costly.

2. It does not require raising IOP to 60mm Hg for microkeratome.

3. This delicate procedure shall be cheapest and can be used by an expert hand.

4. Very high myopia, hypermetropia, astigmatism and presbyopia can be corrected.

5. It does not require a corneal flap to be raised.

V. DISADVANTAGES

1. It is time consuming.

2. Learning curve much higher that LASIK or SMILE procedure.

VI. CONCLUSION

Manual correction of myopia, hypermetropia, astigmatism and presbyopia is simplest, cheapest and reliable. If 1 mm of cornea is tucked, then it corrects **3.174 D** & If 1 mm of horizontal diameter of cornea is reduced, then it corrects **+4.1D.** Because of use of simple procedure to split the cornea, tie the sutures either to tuck it or use of purse string suture to squeeze the horizontal length of cornea, correction of very high myopia, hyprmetropia, astigmatism and presbyopia, this procedure has lots of promises in future.

REFERENCES

[1] Lovisolo,CF, Reinstein DZ; Reinstein(Nov-Dec 2005)"Phakic intraocular Lenses."Survey of Ophthalmology.50(6):549-87.

[2] Sanders DR, Vukich JA; Vukich (May 200K),"Comparison of Implantable Contact Lens and Laser Assisted In Situ keratomileusis for moderate to High Myopia."Cornea 22(4):324-334.

[3] Le vinson,B.A;Rapuano,CJ;Cohen EJ:Hammer Smith K.M.;Ayres B.D; Laibson, PR(2008)."Referrals to the Wills Eye Institute Cornea Service after laser in situ keratomileusis: reasons for patient dissatisfaction."Journal of Cataract & Refractive Surgery 34(1).

[4] Jabbur,N.S;Saktani,K;O'Brien,T.P.(2004)."Survey of Complications and recommendations for management in dissatisfied patients seeking consultation after refractive surgery."Journal of Catarcat and Refractive surgery.30(9):1867-74.

[5] Carrillo C,Chayet AS,Dougherty PJ,Montes M,Magallanes R,Najman J,Fleitman J,Morales A(2005)."Incidence of complications during flap creation in LASIK using the NIDEK MK-2000 microkeratome in 26,000 cases." J Refract Surg.21(5 Suppli):S 655-7.

[6] Eye surgery Education Council."Lasikinstitute.org.Archived from the Original on 2011-09-28.Rerived 2011-12-10.

[7] "Eye Surgery Education Council."Lasikinstitute.org.Archived from the Original on 2011-09-28.Retrieved 2011-12-10.

[8] Tham VM,Maloney RK(May 2000)."Microkeratome complications of laser in situ keratomileusis"Ophthalmology,107(5):920-4.

[9] Vesauloma M,Perez-Santoria J,Petroll WM,Linna T,Alio J,Terro T(1 February 2000)."Corneal Stroma changes included by myopic LASIK."Invest.Ohthalmol.Vis.Sci.41(2)369-76.

Synthesis and Properties of Asymmetric Polyamidosulfoimides on the Basis of Dichloroanhydrides of Saccharin-5-Carboxylic Acids and Aliphatic Diamines

Farah M. Mamedaliyeva

Institute of Polymer Materials of Azerbaijan National Academy of Sciences, Sumgait

Abstract**—** *By polycondensation of dichloroanhydride of saccharin-5-carboxylic acids with aliphatic diamines in dimethylacetamide at room temperature the asymmetric polyamidosulfoimide has been synthesized. The influence of nature of solvent, concentration of the initial reagents and reaction temperature on value of characteristic viscosity and also on solubility, thermal stability and deformation-strength properties of the synthesized polyamidosulfoimides has been investigated. It has been elucidated that a growth of a quantity of methylene groups in the polymer leads to the improvement of solubility of the polymers in dimethylformamide and dimethylacetamide, but at the same time leads to the relative deterioration of thermal stability.*

Keywords**— aliphatic diamines, dichloroanhydride of saccharin-carboxylic acids, polyamidosulfoimide, saccharin-5-carboxylic acid.**

I. INTRODUCTION

In recent years, in the field of chemistry of high-molecular compounds, special attention is paid to the development of methods for the synthesis of high-thermostable polymers [1]. The aromatic and aliphatic polysulfoimides (polysaccharins) are the sulphur-containing analogs of polyimides. The polysulfoimides are differed from polyimides by availability of one carbonyl (C=O) and one sulfonyl (-SO_2-) group in imide cycle. These polymers possess high thermal stability (500-650˚C), solubility, resistance to radiation, light, acidic and alkaline hydrolysis.

In this connection, taking into account the advantages of polysaccharins, it is appeared a need of development of the effective methods for synthesis of new monomers on the basis of saccharin-monocarboxylic acids.

It was known that due to solubility in amide solvents and sufficiently high mechanical, thermal and dielectrical properties the polyamidoimides find a wide application in microelectronics in creation of foil-coated dielectrics as the protective coatings. The polyamidoimides prepared on the basis of dichloroanhydrides of dicarboxylic acids possess sufficiently high molecular weight and are differed with thermal stability and also good physical-mechanical properties [2]. There are data about development of method of synthesis of the polyamidoimides containing side carboxyl groups by interaction of imide-containing dichloroanhydrides of dicarboxylic acids with aromatic diamines [3]. We have previously synthesized the symmetric polyamidosulfoimides on the basis of dichloranhydride of saccharin-6-carboxylic acid and aliphatic and also aromatic diamines [4-6].

The purpose of work – synthesis of asymmetric polyamidosulfoimides (PASI) on the basis of dichloranhydrides of saccharin-5-carboxylic acids and aliphatic diamines.

II. EXPERIMENTAL TECHNIQUE

2.1 Synthesis of polyamidosulfoimides

1,2g (0,02 mol) of ethylene diamine and 4,04g (0,04 mol) of triethylamione dissolved in 50ml of DMFA was placed into flask. Then it was added on portions 6,82g (0,02 mol) of dichloranhydride of saccharin-5-carboxylic acid. The reaction was carried out at room temperature for 3 h. At the end of the reaction, the precipitate of hydrochloric triethylamine was filtered, washed with distilled water, the polymer was precipitated by alcohol, then by acetone and was dried in vacuum to constant mass. The polyamidopsulfoimides on the basis of tetramethylenediamine and hexamethylenediamine have been analogously synthesized.

2.2 Film preparation

The polyamidosulfoimide films have been prepared from polymer solutions in dimethylformamide; the polymer solution was poured on glass surface and dried at room temperature for 10 h, then was subjected to thermal treatment.

The infrared spectra were taken on IR-Fourier-spectrometer LUMOS (firm BRUKER, Germany) within the range of wave frequencies 4000-600 cm^{-1}, with use of attachment NPVO with crystal ZnSe. A diameter of crystal – 1 cm. A number of scans of the sample –24, measurement duration – 30 s.

The curing process was studied by a method of differential-thermal analysis on derivatograph "Paulik-Paulik-Erdei". The sample hanging – 200 mg, sensitivity of channels – TG-200, DTA-250 μv, DTG-1 mv and temperature rise rate – 5°C /min in current air.

III. RESULTS AND DISCUSSION

For synthesis of the polyamidosulfoimides it was used the method of low-temperature polycondensation in the solvents of amide type, as a result of which the polymers of linear structure with alternating sulfoimide and amide groups in the elementary links have been prepared. The initial reagents for preparation of PASI were dichloranhydride of saccharin-5-carboxylic acid and aliphatic (ethylene-, tetramethylene- and hexamethylene) diamines. The reaction proceeds on the following scheme:

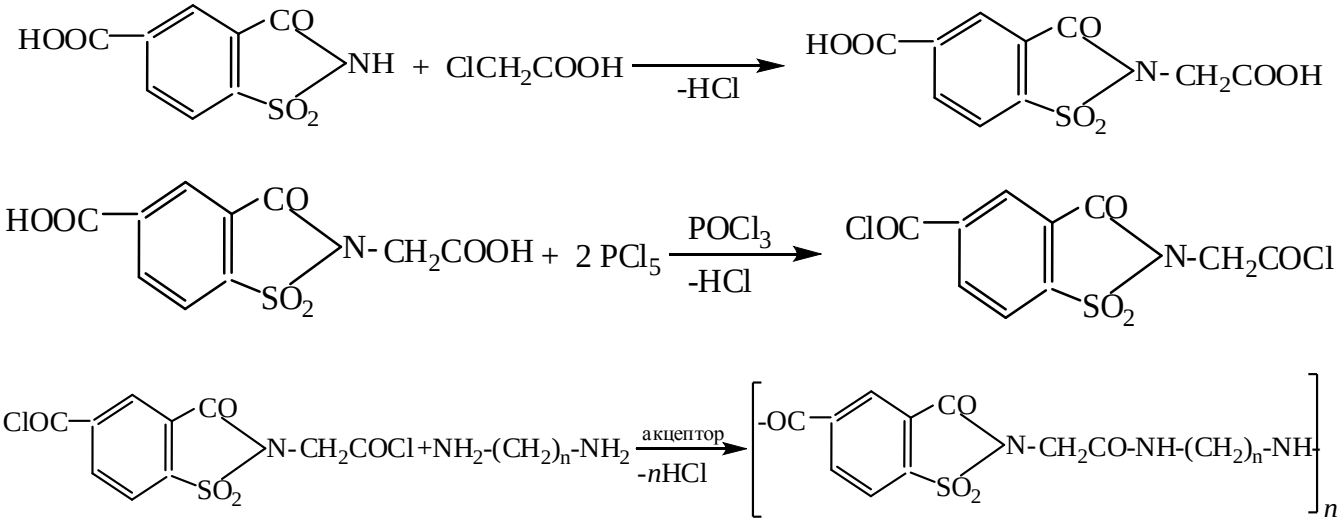

where n=2,4,6

The composition and structure of PASI have been determined by elemental analysis and IR-spectroscopy.

It has been detected that in the IR-spectra of the synthesized compounds there are the absorption bands in the field of 1679 and 1243 cm^{-1}, there are the absorption bands in the field of 3217-3100 cm^{-1}characteristic for >NH group; deformation (739, 861 cm^{-1}) vibrations of C–H bond of substituted benzene ring; deformation (1459 cm^{-1}) vibrations of benzene ring. The absorption in the field of 1721 cm^{-1} is characteristic for C=O bond of carboxylic group. The absorption bands in the field of 1355 cm^{-1} and 1185-1150 cm^{-1}, characteristic for valence vibrations of $–SO_2–$ group in sulfoamides are also observed [7,8]. The valence vibrations at 1298 cm^{-1} are characteristic for C-N bond [7].

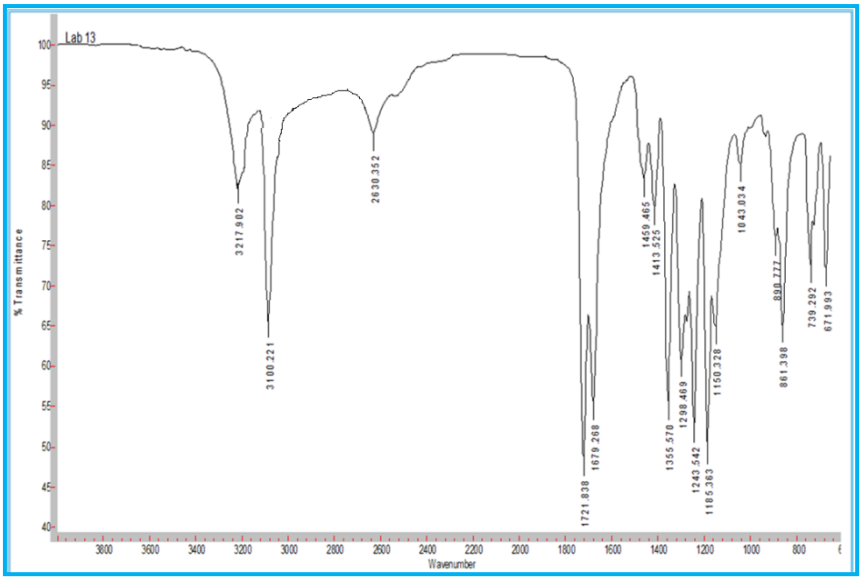

FIGURE 1 . IR SPECTRA OF POLYAMIDOSULFOIMIDES ON THE BASIS OF DICHLOROANHYDRIDES OF SACCHARIN-5-CARBOXYLIC ACID AND ALIPHATIC DIAMINES

The prepared polyamidosulfoimides are the powdery product of yellow color.

It has been investigated the influence of nature of solvent, concentrations of the initial reagents and reaction temperature on value of characteristic viscosity [η]. It has been established that the polymers with the highest viscosity are formed in a medium of dimethylacetamide (DMAA). In this connection, the further polycondensation was carried out in a medium of DMAA.

The nature of the acceptor has also an essential influence on molecular weight of the forming polymer:

Acceptor HCl:	DMAA	Pyridine	$(C_2H_5)_3N$	Na_2CO_3
[η], dl/g	0,22	0,23	0,30	0,55

It was known that DMAA and pyridine are used as the acceptors, but as the carried out investigations showed they are not active enough, as evidenced by the relatively low values of [η]. An application of triethylamine doesn't lead to the polymer preparation with high viscosity, which can be explained by formation of the stable complex of chloranhydride group of DCSCA in DMAA with triethylamine, which complicates the polyamidation. The polyamidosulfoimide with the greatest [η] has been prepared in use of sodium carbonate as an acceptor.

The results of the carried out experiments showed that the highest value of viscosity of the polyamidosulfoimide is reached at 15-20°C. The carrying out of process at lower (5°C) or higher (35-40°C) temperatures leads to a considerable decrease of characteristic viscosity of the polymer. Apparently, this has been connected with stability of complex, forming by chloranhydride group with solvent. At low temperatures this complex is so stable that the reaction with diamine becomes difficult, and at high temperatures the reactive complexes are not generally formed [8].

A concentration of the initial monomers shows also a definite influence; the best values of PASI: [η] 0,51 dl/g (III) have been obtained at concentration of the initial components – 12 mass% (III).

Thus, the optimal conditions of synthesis of the polyamidosulfoimides are as follows: solvent – DMAA, acceptor – sodium carbonate, synthesis temperature – 20°C, reagents concentration – 10-12 mass%. The characteristics of PASI (I- III is presented in Table 1.

It has been found by the methods of DTA and TGA that the decomposition process for these polymers depending on structure for PASI, prepared on the basis of saccharin-5-carboxylic acid is begun at 348-360ºC, and on the basis of saccharin-6-carboxylic acid – at 358-373ºC [9]. The thermogravimetric analyses of the polymer showed that 10%-s mass loss occurs at 385-395ºC (I-III) [10]. On thermal stability the synthesized polyamidosulfoimides depending on used diamine are located in

the following series: ethylene diamine>tetramethylene diamine>hexamethylene diamine.

TABLE 1

SOME CHARACTERISTICS OF THE POLYAMIDOSULFOIMIDES OF COMPOSITION I-III

Polymer	R	Yield, %	[η], dl/g	M.p.,°C	$T_{begin.decom.}$,°C
I.	—$(CH_2)_2$—	80.0	0.46	243	360
II	—$(CH_2)_4$—	82.0	0.48	225	355
III.	—$(CH_2)_6$—	84.0	0.51	207	348

where, I, II, III – data for PASI on the basis of saccharin-5-carboxylic acid

On the basis of synthesized compounds the polyamidosulfoimide films have been prepared. In Table 2 the deformation-strength properties of films prepared from industrial polyamides of composition polyamidoimide-polyvinyl pyrrolidone (PAI-PVP) and synthesized polyamidosulfoimides are presented 2.

TABLE 2

DEFORMATION-STRENGTH PROPERTIES OF FILMS OF COMPOSITIONS I-III AND PAI-PVP

Polymer	R	σ_p, MPa	Δ_ℓ, %
I.	—$(CH_2)_2$—	60	6
II.	—$(CH_2)_4$—	58	8
III.	—$(CH_2)_6$—	55	10
PAI-PVP	–	40	30

As is seen from Table 2, the synthesized polyamidosulfimides on physical-mechanical indices [11] are on the level of the industrial polyamidoimides. These polymers possess also highly film-forming properties.

We have also studied the solubility of the synthesized polyamidosulfoimides in various aprotonic solvents – dimethylformamide and dimethylacetamide. As shown by the results of investigations, the growth of quantity of methylene groups in the polymer leads to the improvement of the polymer solubility, but at the same time, leads to the relative deterioration of the thermal stability.

The synthesized polyamidosulfoimides can be used in electrotechnics as the high-strength coatings holding high temperature regime.

IV. CONCLUSIONS

By polycondensation of dichloroanhydride of saccharin-5-carboxylic acids with aliphatic diamines in dimethylacetamide at room temperature the asymmetric polyamidosulfoimide has been synthesized. It has been established the optimal condition of synthesis of the polyamidosulfimides: solvent – DMAA, acceptor – sodium carbonate, synthesis temperature – 20°C, reagents concentration – 10-12 mass%.

It has been elucidated by methods of DTA and TGA that on thermal stability the prepared compounds depending on used diamine are located in the following series: ethylene diamine>tetramethylene diamine>hexamethylenje diamine. It has been established that the synthesized polyamidosulfoimides possess high physical-mechanical indices. On exploitation indices they are on the level of the industrial polyamidoimides. It has been revealed that the growth of quantity of methylene groups in the polymer leads to the improvement of the polymer solubility in aprotonic solvents, but also to the relative deterioration of their thermal stability.

REFERENCES

[1]. E. T. Aslanova, F. M. Mamedaliyeva, T. A. Aslanov, and B. A. Mamedov, "Synthesis of Symmetrical Polyamide–Sulfonimides Based on Bis-saccharin Dicarboxylic Acid Dichlorides," Russian Journal of General Chemistry, vol. 89, pp. 96-99, January 2019.

[2]. Yu. A. Mikhaylin, Thermostable polymers and polymer materials, SPb.: Professiya, 2006, 623 s.

[3]. M. Y. Goyxman, I. B. Podeshvo, and G. M. Mixaylov, "New bifunctional monomer – dichloroanhydride of terephthaloil-bis-(3-methoxy-4oxybenzoic) acid and poliimides on its basis," Russian Journal of Applied Chemistry, vol. 70, pp. 312-326, February 1997/

[4]. T. A. Aslanov, M. S. Salakhov, and A. A. Efendiev "Poly(amide sulfimides) based on disaccharincarboxylic acid dichlorides and diamines," Polymer Science. Series B, vol. 47, pp.68-71, March-April 2005.

[5]. T. A. Aslanov, "Synthesis of polyamido(ether)sulfoimides by a method of polycondensation", Azerb.Chem.J., pp. 116-122, April 2005.

[6]. T. A. Aslanov, E. T. Aslanova, F. M. Mamedaliyeva, and N. Y. Ishenko, "Synthesis of imide 4-sulfoizophthalic acid and its some amide derivatives", Azerb.Chem.J., pp. 54-58, March 2015.

[7]. B. N. Tarasevich, IR spectra of main classes of organic compounds. Resource materials," M.: MSU, 2012, 55p.

[8]. I. I. Osovskaya, and V. S. Antonova, Viscosity of polymer solution. Text book, Sankt-Peterburq, 2016, 61 p.

[9]. V. F. Kurenkov, Practicum on chemistry and physics of polymers, M.: Khimiya, 1990, 299 p.

[10]. I. P. Petryuk, A. N. Gaydadin, and S. A. Efremova, Determination of kinetic parameters of thermodestructive polymer materials on data of dynamic thermogravimetry, Volqoqrad: Volq GTU, 2010. 16 p.

[11]. A. G. Voronkov, and V. P. Yarchev, Investigation of physical-mechanical properties of polymers and polymer compositions, Tambov: Publ.Tambov State Technological University, 2004, 28p.

Approximate 3-D model for analysis of laminated plates with arbitrary lay-ups, loading and boundary conditions

Andrea Urraci[1], Ugo Icardi[2]

Dipartimento di Ingegneria Meccanica e Aerospaziale, Politecnico di Torino, Italy

Abstract**—***Available exact solution techniques of elasto-static problems entail limitations on the choice of lay-ups, loading and boundary conditions and impose restrictions on strain and stress fields as well, to overcome algebraic difficulties inherent to modeling of laminated and sandwich composites. Therefore in fact they become unsuitable for testing accuracy of modern laminated plate theories aiming to very accurately describing 3-D stress fields in real conditions of use of multilayered composites, nowadays widespread in engineering applications. To overcome the assumption of too restrictive hypotheses, an approximate 3-D solution technique is proposed and assessed that is able to automatically solve problems which due to the lay-ups, loading and boundary conditions assumed would not be solved with the exact techniques available. A quite general, accurate structural model is developed that comes to constitute a generalization of available physically-based zig-zag theories, being free from through-thickness assumptions and because zig-zag functions are not explicitly contained, the layerwise contributions being represented by the redefinition of coefficients of the through-thickness series expansion. It is based solely on the prescriptions of the theory of elasticity, i.e., displacement and stress compatibility at interfaces, fulfillment of local equilibrium equations at points across the thickness and of stress boundary constraints. A truncated expansion series of trial functions and unknown amplitudes is used to represent variables, whose coefficients are determined in exact form using a symbolic calculus tool that enforces all elasticity constraints and in conjunction with Rayleigh-Ritz and Lagrange multipliers methods.*

Keywords**—Composite and sandwich plates, zig-zag theories, interlaminar transverse shear/normal stress continuity, localized and distributed loadings, FEA 3-D, elastostatic solutions.***

I. INTRODUCTION

Laminated and sandwich composites are progressively replacing traditional metallic materials in various engineering applications, thanks to their superior properties in terms of specific strength and stiffness, energy absorption, fatigue and corrosion properties.

Due to strongly different in-plane and transversal elastic properties that distinguish these materials, 3-D stress fields take place that condition formation and growth of local damage and failure mechanisms and that require specific structural models. The main aspect to highlight is that their displacement field must be C°-continuous (zig-zag effect), so that appropriate slope discontinuities occurs and consequently local equilibrium equations can be satisfied at layer interfaces. A multitude of theories is to date available that differently account for the mentioned layerwise effects and which so have a different order of accuracy and different computational costs. A broad discussion of this matter is given by Carrera and co-workers [1-4], Vasilive and Lur'e [5], Reddy and Robbins [6], Lur'e, and Shumova [7], Noor et al. [8], Altenbach [9], Khandan et al. [10] and Kapuria and Nath [11] and in the book by Reddy [12].

Due to the inevitable limiting hypotheses a priori formulated, laminated plate theories may no longer be accurate for arbitrary lay-ups, loading and boundary conditions and strong transverse anisotropy that are typical of some practical applications. As most of the assessments have been carried out just considering cross-ply lay-ups, sinusoidal heap loading and simply-supported edges, since exact solutions can be determined and used for comparisons, and unfortunately usually a mild variation of thickness and elastic properties of layers, what the limits of available theories may be is not well known in general.

Exact solutions, of which by way of example the papers by Brischetto [13] (static analysis of multi-layered plates and shells), Yang et al. [14] (free vibration analysis of laminated, box and sandwich Icardi [15] (exact solution for a damaged sandwich beam with laminated faces) and by Ren [16] (laminated shell in cylindrical bending) are cited, usually assume thin constituent layers in order plane strain conditions can be postulated. In addition, they assume symmetric lay-ups, simply-supported conditions and sinusoidal loading, because solutions can be assumed in trigonometric form. Then, stresses are

assumed across the thickness and strain compatibility is enforced, in accordance with Pagano [17,18] who pioneered the technique for finding exact solutions.

The algebraic complexity forced researchers to take on the previous assumptions, but they cannot be appropriate for exhaustively testing theories and their finite elements, as is evident. Clamped edges, layers with very different material properties and thickness and localised distributed loading should instead be considered since they are more probative, as highlighted by the results of theories in disagreement with each other [19-21] for the cited cases, while under conditions that enable the existence of exact solutions they agree. So approximate, but yet accurate, 3-D, closed form solutions (theoretical foundations comprehensively discussed by Reddy and Chao [22] and Yakimov [23]) suitable for arbitrary assumptions have to be considered to test theories and finite elements. Consequently approximate closed form approaches must be applied whose variables are expressed as a truncated series expansion of assumed trial functions, the related unknown amplitudes being determined using e.g. Rayleigh-Ritz method, provided that restrictive assumption that can nullify the desired generality are not introduced.

It must be considered that 3-D FEA cannot be reliable under arbitrary assumptions of loading and boundary conditions and therefore cannot be considered as the only comparison result for theories, because elements in displacement-based form do not exactly satisfy local equilibrium equations, while mixed finite elements [24] may be affected by geometric and material singularity edge effects and anyway both may be strongly influenced by local effects of loading and constraints.

A tool that can be used to prevent the need of assuming restrictive hypotheses to overcome the algebraic difficulties inherent to the development of a quite general structural model is symbolic calculus. Although one would expect a widespread use of this tool, at the best of authors' knowledge still no applications of it (except [19-21]) is available in the nowadays literature, despite it is particularly suitable for easily manipulating the intricate algebraic passages that follows when arbitrary loading and boundary conditions are assumed.

Aiming to avoid having to assume too restrictive hypotheses dictated by algebraic difficulties when solving structural problems of laminated and sandwich composites (the latter being assumed in homogenized form as a set of layers with very different properties) with quite general lay-up, elastic moduli, loading and boundary conditions, in the present paper the structural models [19-21] across the thickness and their (for the truth few and not too much restrictive) hypotheses are replaced with a general representation of variables, which is able to capture the salient aspects while minimizing computational costs, so to provide a quick and accurate tool that furnishes a 3-D solution of comparison. The purpose is to develop an approximate but accurate 3-D solution which does not introduce simplifying a priori hypotheses about through-thickness kinematics, strain and stress fields, which respects all physical and elasticity constraints and so which comes to constitute a generalization of zig-zag theories [19-21] that likewise uses a fixed number of d.o.f. irrespective of the number of layers. No zig-zag layerwise functions are incorporated, the coefficients of the displacement field playing the role of layerwise functions themselves being redefined across the thickness through the enforcement of physical constraints. The latter are constituted by interfacial stress and displacements compatibility, by stress boundary conditions, by local equilibrium equations at points across the thickness, as well as physical constraints specifying the nature of solutions within the domain. The characteristic feature is that all constraints are satisfied in exact form through use of a symbolic calculus tool that provides once and for all expressions deriving from the enforcement of constraints.

The analytical solution is searched as a truncated expansion series of trial functions and unknown amplitudes (like, e.g. Vel and Batra [25]) using Rayleigh-Ritz method, the kinematic avariables constituting the unknowns being expanded in the in- and out-of-plane directions, a structural model that is configured in advance being lacking. As a consequence, the proposed approach assumes characteristics similar to the search for closed form solutions using laminated plate theories [22,23]. But, at the same time, it is similar to the search of exact solutions [13-18], given the lack of a structural model assumed a priori and the imposition of wanted characteristics to solutions. So, ultimately, the solution is configured through the choice of the constraints imposed, consequently it can be changed at will by the user in the applications. The crucial difference is that enforcements are solved via symbolic calculus, thus allowing for more general situations. In particular, the load can be arbitrarily chosen, it being expressed as an analytical function of the coordinates that is managed exactly. Anyway, the solution is get automatically and quickly by the symbolic calculus tool, irrespective of the choices made. A number of challenging benchmarks with strong layerwise effects are considered in the applications (see Tables 1 and 2) to demonstrate accuracy and efficiency of the proposed approach. Results by3-D FEA [24], by multilayered theories with different characteristics retaken from [20,21] and exact solutions, where available, are used for comparisons.

TABLE 1
GEOMETRY, LOADING AND BOUNDARY CONDITIONS.

Case	Layer thickness	Material		Loading	Lx/h	Ly/Lx
a	[(2h/7) / (4h/7) / (h/7)]	[n/n/n]	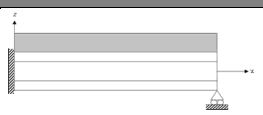	$p^0(x) = p^0_u$ if $0 \le x \le L_x$	14.286	-
b	[$(h/3)_3$]	[p_3]		$p^0(x) = p^0_u \sin(\pi x / L_x)$ if $0 \le x \le L_x$	4	-
c	[$(h/3)_3$]	[c1/c1/c1]	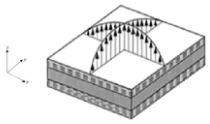	$p^0(x,y) = p^0_u \sin(\pi x / L_x)\sin(\pi y / L_y)$ if $0 \le x \le L_x$ and $0 \le y \le L_y$	4	3
d	[0.1h / 0.4h]$_S$	[Gr-Ep/Foam]$_S$	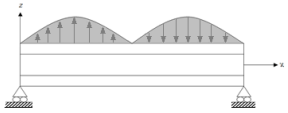	$p^0(x) = p^0_u \sin(2\pi x / L_x)$ if $0 \le x \le L_x$	10	-
e	[0.1h_2/0.2h_3/0.1h_2]	[pf_2/pvc/hh/ pvc/pf_2]	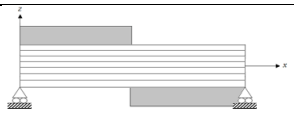	$p^0(x) = \begin{cases} p^0_u & \text{if } 0 \le x \le L_x/2 \\ -p^0_u & \text{if } L_x/2 \le x \le L_x \end{cases}$	8	-
f	[0.2h/0.7h/0.1h]	[c2/c2/c2]	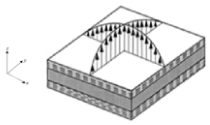	$p^0(x,y) = p^0_u \sin(\pi x / L_x)\sin(\pi y / L_y)$ if $0 \le x \le L_x$ and $0 \le y \le L_y$	4	3

TABLE 2
MECHANICAL PROPERTIES

Material name	c1 [iso]	c2 [iso]	Foam	Gr-Ep	hh	n [iso]	p	pf	pvc
E1[GPa]	-	-	0.035	132.38	0.250	-	172.4	25000	250
E2[GPa]	-	-	0.035	10.76	0.250	-	6.89	1000	250
E3 [GPa]	M1	M2	0.035	1.076	2.5	M3	6.89	1000	250
G12 [GPa]	-	-	0.0123	5.65	0.001	-	3.45	500	96.2
G13 [GPa]	-	-	0.0123	5.65	0.875	-	3.45	500	96.2
G23 [GPa]	-	-	0.0123	3.61	1.750	-	1.378	200	96.2
υ12	0.34	0.34	0.4	0.24	0.9	0.33	0.25	0.25	0.3
υ13	0.34	0.34	0.4	0.24	$3x10^{-5}$	0.33	0.25	0.25	0.3
υ23	0.34	0.34	0.4	0.49	$3x10^{-5}$	0.33	0.25	0.25	0.3
M1 E_l/E_u=5/4, $E_l/E_c=10^5$; M2 E_l/E_u=5/4, $E_l/E_c=10^4$; M3 E_u/E_l=1.6, $E_u/E_c=166.6\cdot10^5$; [iso]=isotropic $E_1=E_2=E_3$ $G_1=G_2=G_3$									

II. THEORETICAL FRAMEWORK

Hereafter requirements of the present approximate 3-D solution approach and its peculiar features across the thickness, notations, the solution technique itself, in-plane representations used in each single case and the relative order of expansion are discussed in sequence.

2.1 Requirements

Layers are assumed to have linear elastic anisotropic properties, which may be distinctly different from one another, in addition, they may have a different thickness, to enable considering a strong transverse anisotropy.

In accordance with the intended aim of this paper, the following further requirements must be respected.

With regard to stress fields, no restrictive a priori assumptions are made, except out-of plane components and also the through-thickness gradient of the transverse normal stress must be continuous at interfaces, as prescribed by the elasticity theory. Self-equilibrated stress fields are not assumed a priori, since the equilibrium is satisfied in approximate integral form within the governing functional and in point-format few selected points across the thickness. Stress-free boundary conditions on upper and lower bounding faces are identically satisfied within the symbolic calculation process, but any other arbitrary condition of interest could be freely imposed in accordance with the chosen loading.

Displacements could be assumed to be either continuous or discontinuous (so to use cohesive models, e.g. for studying delamination) at interfaces. However, in the present case the choice is limited to the first option. No restriction is made about the order and therefore to the number of coefficients of the expansion representing displacements across the thickness (1), it being determined by the number of constraints that one intends to impose case by case. As will be specified below, in numerical applications a low but sufficiently accurate order of expansion is chosen, which the same for each layer is. As well, any kind of in-plane representation can be used.

Here the Total Potential Energy functional (TPE) is chosen as governing functional, loadings being conservative, which is solved in a discrete form using Rayleigh-Ritz method, although any other functional could be used to find the solution in conjunction with a symbolic calculus tool.

In fact, like for any other assumption of the procedure, it is sufficient expressing the relative formula, then the calculation proceeds automatically.

2.2 Notations

A Cartesian coordinate reference system (x, y, z) is assumed as the reference frame, (x, y) representing the reference plane Ω and consequently z being the thickness coordinate. The position of Ω can be assumed arbitrarily across the thickness, so to avoidthe possible zeroing of coefficients at z=0 for certain lay-ups and assumed forms of solution.

Tensor notation is used to make formulas compact, so symbols x, y, z can be replace by Greek letters, i.e. $\alpha = 1,2 \equiv x, y$; $\varsigma = 3 \equiv z$, then Einstein summation convention is used. A comma is used to indicate spatial derivatives, e.g. $(.)_{,x} = \partial / \partial x$, $(.)_{,z} = \partial / \partial z$).

The overall thickness of the laminate is indicated by *h*, whileLx and Ly symbolize the plate side-length in the x- and y-directions. Layers are assumed to have uniform thickness h^k and to be perfectly bonded to each other (bonding resin interlayer disregarded).

To symbolize that a quantity belong to a specific layer, e.g. k -th one, subscripts $_k$ or superscripts ^{k} are affixed, while ^{u} and $_l$ indicate that quantities are evaluated at upper or lower faces of the laminated structure, respectively. Accordingly, $^{(k)}z^+$ and $^{(k)}z^-$ represent the thickness coordinates just after or just before the interface *k*, respectively.

Strains, which are assumed to be infinitesimal, and stresses are symbolized respectively by ε_{ij} and σ_{ij} , while in-plane and transverse components of elastic displacements are indicated as u_α and u_ς .

The functional d.o.f. are represented by the coefficients constituting the amplitudes of the series expansion of displacements. Because a fixed representation (namely, shape and order) is used across each constituent layers. Characteristic feature, coefficients are recalculated layer by layer by enforcing constraints (see section 2.3.1). As a consequence, the number of d.o.f. does not depend depends on the number of constituent layer (as will be specified in detail below).

Because the representation is the same for each layer but coefficients are re-calculated, the displacement field will be affected by an index ^{J} representing the counter of computational layers, whose number can be equal, greater or lower than the number of physical layers *k*.

2.3 Structural model

The following displacement field is postulated across the thickness:

$$u_{\alpha}{}^{j} = \sum_{k=0}^{n_{\alpha}} \sum_{p=1}^{P} \sum_{m=1}^{M} \left[{}_{p\,m}{}^{j}a_{k}^{\alpha}\left(x,y\right) z^{(k-1)} \right]$$
$$u_{\varsigma}{}^{j} = \sum_{k=0}^{n_{\varsigma}} \sum_{p=1}^{P} \sum_{m=1}^{M} \left[{}_{p\,m}{}^{j}b_{k}^{\alpha}\left(x,y\right) z^{(k-1)} \right] \quad (1)$$

It could be noticed that that it is a completely generic representation and therefore is characterized by the absence of restrictive assumptions across the thickness, at the contrary of laminated plate models.

Instead of introducing a priori assumptions like in the plate models, here the behavior of the structure is described by the imposition of the appropriate physical constraints that come to characterize the behavior of the structure within the domain (here means across the thickness) and at the boundary, as outlined forward. Therefore (1) constitutes the approximate solution of the resulting boundary value problem that will be discussed in detail below.

The representation chosen (1) is the product of truncated series expansions, respectively in (x, y) and z (where z is calculated starting from Ω), whose coefficients are the unknowns, namely the functional degrees of freedom. In-plane expressions of contributions ${}_{p\,m}{}^{j}a_{k}^{\alpha}\left(x,y\right)$ and ${}_{p\,m}{}^{j}b_{k}^{\alpha}\left(x,y\right)$ are chosen to fulfill constraint conditions on the lateral boundary surface of the laminated structure under examination, so, trial functions a priori individually satisfy the prescribed boundary conditions, where M and P are the maxim expansion order through in-plane directions.

Amplitudes ${}_{p\,m}{}^{j}a_{k}^{\alpha}$ and ${}_{p\,m}{}^{j}b_{k}^{\alpha}$ are determined once and for all by the symbolic calculus tool used through the contemporary application of Rayleigh-Ritz, Lagrange Multipliers methods, by stress boundary conditions at upper and lower bounding faces, as well as by imposing the satisfaction of interfacial displacements and stress conditions and the fulfillment of local equilibrium equations at points selected across each computational ^{J} or physical layer $^{J=i}$.

However, even if the solution search methodology is classic, the use of symbolic calculus makes it worthy of note, owing to its peculiar characteristics. Indeed, symbolic calculus enables the simultaneous imposition of local equilibrium equations, interfacial displacement and stress compatibility conditions across the thickness (which can be chosen and changed at the discretion of the operator, as the calculation proceeds anyway automatically) and an arbitrary choice of loading obtaining in any case quickly and once and for all the exact relationships among involved quantities, without having to resort to restrictive assumptions to overcome the complexity of the calculation, as would happen by hand.

As mentioned above in 2.2, Ω can be chosen at any position across the thickness and then changed as desired by the user, because symbolic calculus tools finds always the same solution irrespective for this choice, provided that the set of physical constraints remains the same. In this way it is prevented that stresses are erroneously predicted to vanish for z=0 due to the possible, although unlikely (given the high degree of generality), zeroing of coefficients that could occur in some cases. So, it is not necessary to include any zig-zag functions or define a specific role or position for any coefficients. Results of the present theory (1) with two different reference frames are reported for case a.

The unknown amplitudes, which constitute the d.o.f. of the problem, are fixed in number because they just depend on the expansion order chosen a priori across the thickness of each layer, which is assumed the same for all layers (n_{α} and n_{α}) and by in-plane expansion orders M and P . Expressions coming from the enforcement of the constraints are re-determined for each lamina as functions of the unknowns, that is the amplitudes in (1), whose number depends on the order of expansion chosen and remains fixed. As physical constraints are enforced, the present structural model must be included in the context of physically-based theories.

In this paper, a cubic/forth-order through-thickness representation is assumed because numerical tests revealed this degree of expansion to be appropriate for finding accurate solutions in all the cases considered. It has to be pointed out that that a such expansion order is much lower compared to structural models that are more in vogue today and do not impose physical constraints [1-12]. Therefore a significant advantage is constituted by the fact that imposing all the relevant physical constraints, a low order of expansion is sufficient.

Note that the order of expansion could be exchanged between in-plane and out of plane components (1) without the results changing. Indeed, symbolic calculus finds always the same exact relations among quantities when the same set of constraints

is imposed. It should also be noted that users can freely choose the sequence of what condition (which will be explicitly defined below) to impose first, as well as the functional to be used and the representation since calculations proceed automatically, as already mentioned above.

It is reminded that the final result obtained in this way accounts for the imposition of constraints across the thickness, i.e. the continuity of displacements and stresses (which can be relaxed if desired), stress boundary conditions and local equilibrium equations.

2.3.1 Structural model construction and solution procedure

The construction of the computational model starts by imposing the various constraint conditions starting always from the lower lamina, then it progressively precede up to the upper one and finally the amplitudes are determined by the Rayleigh-Ritz method.

For each layer, as results from (1), there are 13 coefficients to be defined by enforcing physical constraints across the thickness for a cubic/quartic expansion. Therefore an overall number of 13xNxPxM computations is required if in total the layers are N and P and M are the maximal expansion orders along x and y axis respectively.

Before proceeding it is necessary to distinguish the upper and lower layers from ones inside, since the calculation of the coefficients is carried out differently. Note that although the coefficients ${}_{p\,m}{}^{j}a_k^{\alpha}$ and ${}_{p\,m}{}^{j}b_k^{\alpha}$ of (1) do not have a specific a priori fixed role, so they can be determined by exchanging freely the conditions to be enforced for computing each of them, because always the same final result will be obtained, hereafter a specific choice is made in order to explain the procedure.

At interfaces of intermediate layers, the following four stress compatibility conditions [15] are enforced

$$\sigma_{\alpha\varsigma}({}^{(k)}z^{+}) = \sigma_{\alpha\varsigma}({}^{(k)}z^{-});\ \sigma_{\varsigma\varsigma}({}^{(k)}z^{+}) = \sigma_{\varsigma\varsigma}({}^{(k)}z^{-});\ \sigma_{\varsigma\varsigma,\varsigma}({}^{(k)}z^{+}) = \sigma_{\varsigma\varsigma,\varsigma}({}^{(k)}z^{-}) \tag{2}$$

which follows in a straightforward way from local equilibrium equations

$$\sigma_{\alpha\beta,\beta} + \sigma_{\alpha\varsigma,\varsigma} = b_{\alpha} \quad ; \quad \sigma_{\alpha\varsigma,\alpha} + \sigma_{\varsigma\varsigma,\varsigma} = b_{\varsigma} \tag{3}$$

because the derivability of stresses must be guaranteed. The following three displacement continuity conditions must also be enforced at interfaces

$$u_{\alpha}({}^{(k)}z^{+}) = u_{\alpha}({}^{(k)}z^{-});\ u_{\varsigma}({}^{(k)}z^{+}) = u_{\varsigma}({}^{(k)}z^{-}) \tag{4}$$

otherwise as an alternative a suitable cohesive model could be used. Because a total number of 7x(N-1)physical constraints is enforced at each interface through (2) and (4), then 6x(N-1)+13are still undetermined, out of a total of 13xN.

However, 6xN relations could be computed by imposing the fulfillment of (3) at two points arbitrarily chosen across the thickness of the N constituent layers, but in this way the eight boundary conditions (5) could not be satisfied.

Since the first interface has not yet been met when the lower bounding layer is considered, it is impossible to enforce the 7 continuity conditions of stress and displacements discussed above for the first layer, but instead the following 4 boundary conditions

$$\sigma_{\alpha\varsigma} = \sigma_{\varsigma\varsigma,\varsigma} = 0 \ ; \ \ \sigma_{\varsigma\varsigma} = p^{0}(\pm) \tag{5}$$

could be imposed ($p^{0}(\pm)$ is the continuous or discontinuous mathematical function representing the loading acting over the upper^{+} or lower^{-} layers) and the same applies to the upper lamina, because there are no further interfaces to consider. In the present paper, two sets of equilibrium conditions are enforced in the inner layers, while just one is enforced in the outer layers. Once this is done, the remaining free variables, which constitute the d.o.f. (it is reminded that the total number of unknowns is 13xNxPxM, of which P and M depend on in-plane expansion order)are determined using Rayleigh-Ritz method. If a greater number of equilibrium points is needed, it is sufficient to subdivide the physical layer into computational ones.

Because in isotropic beams and plates, which anyway are not the cases for which the present technique is developed, no stress compatibility relations can be enforced being already identically satisfied, a greater number of amplitudes must be determined by the Rayleigh-Ritz method.

2.3.2 Trial Functions

Once constraints are imposed as outlined above, the process continues by assuming appropriate in-plane expressions of coefficients and applying the Rayleigh-Ritz method. The whole solution procedure is summarized in Figure 1.

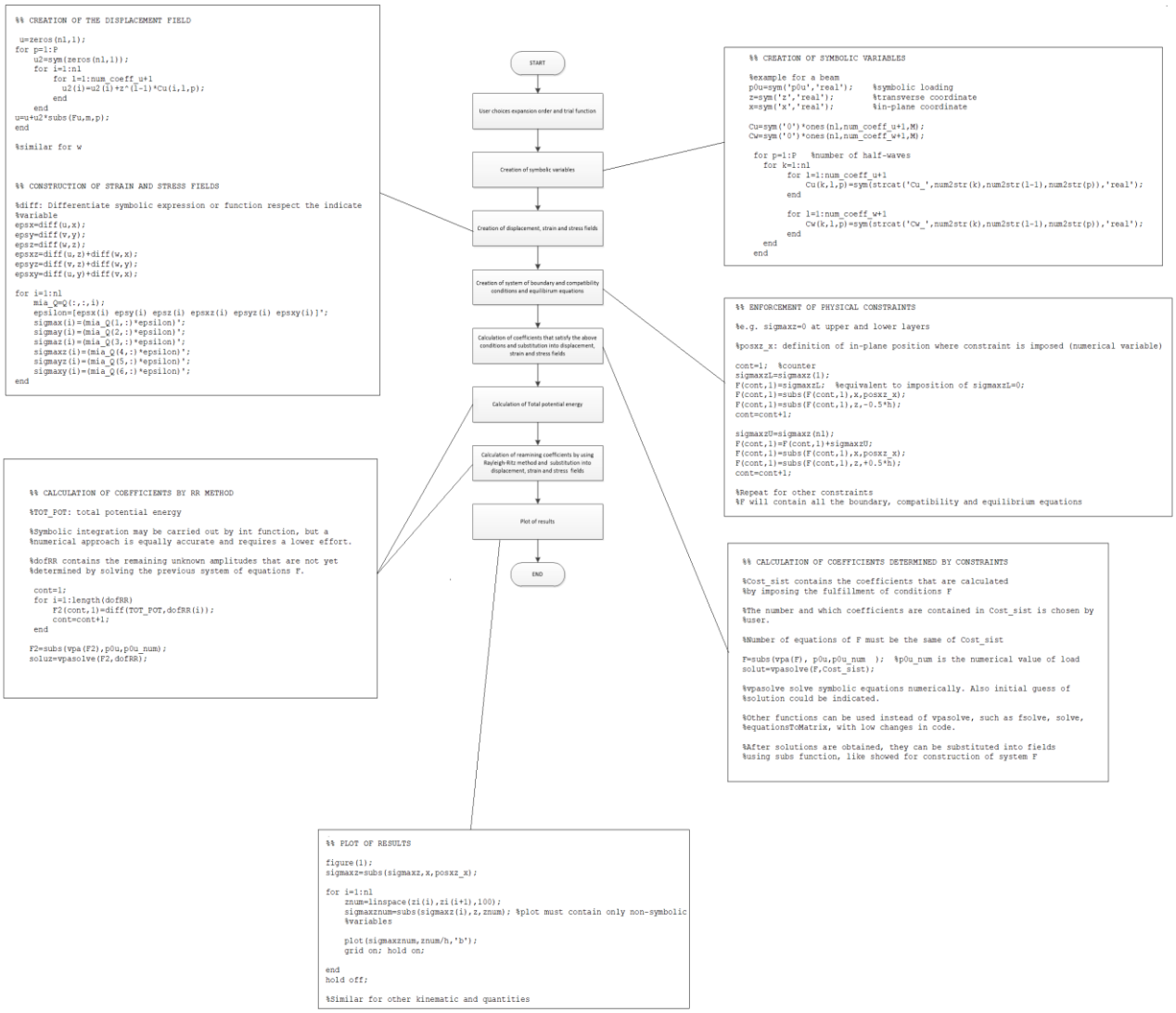

FIGURE 1: Schematic representation of the solution procedure.

If Δ symbolizes in turn ${}_{p\,m}{}^{j}a_k^{\alpha}(x,y)$ and ${}_{p\,m}{}^{j}b_k^{\alpha}(x,y)$ the in-plane contribution to solution (1) is postulated as:

$$\Delta = \sum_{i=1}^{m_\Delta} A_\Delta^i \; \Re^i(x,y) \tag{6}$$

where A_Δ^i are unknown amplitudes and $\Re^i(x,y)$ are trial functions specific to each case, which individually satisfy the prescribed, (also called geometric) boundary conditions, while mechanical also (called natural) boundary conditions are satisfied using Lagrange multipliers method. Table 3 reports the expressions of $\Re^i(x,y)$ for each specific case, along with the expansion order and normalizations used. Trial functions are chosen in order to fulfil the following sets of boundary conditions specific for each of the examined cases.

TABLE 3
TRIAL FUNCTIONS, EXPANSION ORDER AND NORMALIZATION.

Case	Trial functions (6)	Expansion	Normalization
a	$\Re^{m}{}_{\alpha}(x,y)=\left(\frac{x}{L_x}\right)^m$; $\Re^{m}{}_{\varsigma}(x,y)=\left(\frac{x}{L_x}\right)^m$;	9	$\overline{u_\alpha}=\frac{u_\alpha(L_x,z)}{hp^0}$ $\overline{u_\varsigma}=\frac{u_\varsigma(L_x,z)}{hp^0}$ $\overline{\sigma_{\alpha\alpha}}=\frac{\sigma_{\alpha\alpha}(L_x,z)}{p^0(L_x/h)^2}$ $\overline{\sigma_{\alpha\varsigma}}=\frac{A\sigma_{\alpha\varsigma}(L_x,z)}{P^0L_x}$ $\overline{\sigma_{\varsigma\varsigma}}=\frac{\sigma_{\varsigma\varsigma}(L_x,z)}{p^0}$
b	$\Re^{m}{}_{\alpha}(x,y)=\cos\left(\frac{m\pi x}{L_x}\right)$; $\Re^{m}{}_{\varsigma}(x,y)=\sin\left(\frac{m\pi x}{L_x}\right)$;	1	$\overline{u_\alpha}=\frac{E_2u_\alpha(0,z)}{hp^0}$ $\overline{u_\varsigma}=\frac{100h^3E_2u_\varsigma\left(\frac{L_x}{2},z\right)}{L_x^4p^0}$ $\overline{\sigma_{\alpha\alpha}}=\frac{\sigma_{\alpha\alpha}\left(\frac{L_x}{2},z\right)}{p^0}$ $\overline{\sigma_{\alpha\varsigma}}=\frac{\sigma_{\alpha\varsigma}(0,z)}{p^0}$ $\overline{\sigma_{\varsigma\varsigma}}=\frac{\sigma_{\varsigma\varsigma}\left(\frac{L_x}{2},z\right)}{p^0}$
c	$\Re^{m\,n}{}_{\alpha}(x,y)=\cos\left(\frac{m\pi}{L_x}x\right)\sin\left(\frac{n\pi}{L_y}y\right)$; $\Re^{m\,n}{}_{\beta}(x,y)=\sin\left(\frac{m\pi}{L_x}x\right)\cos\left(\frac{n\pi}{L_y}y\right)$; $\Re^{m\,n}{}_{\varsigma}(x,y)=\sin\left(\frac{m\pi}{L_x}x\right)\sin\left(\frac{n\pi}{L_y}y\right)$;	1	$\overline{u_\alpha}=\frac{E_{1\_core}\,u_\alpha\left(0,\frac{L_y}{2},z\right)}{p^0(L_x^3/h^2)}$ $\overline{u_\beta}=\frac{u_\beta\left(\frac{L_x}{2},0,z\right)}{hp^0}$ $\overline{u_\varsigma}=\frac{u_\varsigma\left(\frac{L_x}{2},\frac{L_y}{2},z\right)}{hp^0}$ $\overline{\sigma_{\alpha\alpha}}=\frac{\sigma_{\alpha\alpha}\left(\frac{L_x}{2},\frac{L_y}{2},z\right)}{p^0(L_x/h)^2}$ $\overline{\sigma_{\beta\beta}}=\frac{\sigma_{\beta\beta}\left(\frac{L_x}{2},\frac{L_y}{2},z\right)}{p^0(L_x/h)^2}$ $\overline{\sigma_{\alpha\beta}}=\frac{\sigma_{\alpha\beta}(0,0,z)}{p^0(L_x/h)^2}$ $\overline{\sigma_{\alpha\varsigma}}=\frac{\sigma_{\alpha\varsigma}\left(0,\frac{L_y}{2},z\right)}{p^0(L_x/h)}$ $\overline{\sigma_{\beta\varsigma}}=\frac{\sigma_{\beta\varsigma}\left(\frac{L_x}{2},0,z\right)}{p^0}$ $\overline{\sigma_{\varsigma\varsigma}}=\frac{\sigma_{\varsigma\varsigma}\left(\frac{L_x}{2},\frac{L_y}{2},z\right)}{p^0}$
d	$\Re^{m}{}_{\alpha}(x,y)=\cos\left(\frac{2m\pi x}{L_x}\right)$;	1	$\overline{u_\alpha}=\frac{u_\alpha(0,z)}{hp^0}$ $\overline{u_\varsigma}=\frac{u_\varsigma\left(\frac{L_x}{4},z\right)}{hp^0}$ $\overline{\sigma_{\alpha\alpha}}=\frac{\sigma_{\alpha\alpha}\left(\frac{L_x}{4},z\right)}{p^0(L_x/h)^2}$ $\overline{\sigma_{\alpha\varsigma}}=\frac{\sigma_{\alpha\varsigma}(0,z)}{p^0}$ $\overline{\sigma_{\varsigma\varsigma}}=\frac{\sigma_{\varsigma\varsigma}\left(\frac{L_x}{4},z\right)}{p^0}$
e	$\Re^{m}{}_{\varsigma}(x,y)=\sin\left(\frac{2m\pi x}{L_x}\right)$;	1	
f	$\Re^{m\,n}{}_{\alpha}(x,y)=\cos\left(\frac{m\pi}{L_x}x\right)\sin\left(\frac{n\pi}{L_y}y\right)$; $\Re^{m\,n}{}_{\beta}(x,y)=\sin\left(\frac{m\pi}{L_x}x\right)\cos\left(\frac{n\pi}{L_y}y\right)$; $\Re^{m\,n}{}_{\varsigma}(x,y)=\sin\left(\frac{m\pi}{L_x}x\right)\sin\left(\frac{n\pi}{L_y}y\right)$;	1	$\overline{u_\alpha}=\frac{u_\alpha\left(0,\frac{L_y}{2},z\right)}{hp^0}$ $\overline{u_\beta}=\frac{u_\beta\left(\frac{L_x}{2},0,z\right)}{hp^0}$ $\overline{u_\varsigma}=\frac{u_\varsigma\left(\frac{L_x}{2},\frac{L_y}{2},z\right)}{hp^0}$ $\overline{\sigma_{\alpha\alpha}}=\frac{\sigma_{\alpha\alpha}\left(\frac{L_x}{2},\frac{L_y}{2},z\right)}{p^0(L_x/h)^2}$ $\overline{\sigma_{\beta\beta}}=\frac{\sigma_{\beta\beta}\left(\frac{L_x}{2},\frac{L_y}{2},z\right)}{p^0(L_x/h)^2}$ $\overline{\sigma_{\alpha\beta}}=\frac{\sigma_{\alpha\beta}(0,0,z)}{p^0(L_x/h)^2}$ $\overline{\sigma_{\alpha\varsigma}}=\frac{\sigma_{\alpha\varsigma}\left(0,\frac{L_y}{2},z\right)}{p^0}$ $\overline{\sigma_{\beta\varsigma}}=\frac{\sigma_{\beta\varsigma}\left(\frac{L_x}{2},0,z\right)}{p^0}$ $\overline{\sigma_{\varsigma\varsigma}}=\frac{\sigma_{\varsigma\varsigma}\left(\frac{L_x}{2},\frac{L_y}{2},z\right)}{p^0}$

At simply-supported edges, the following boundary conditions are enforced at $x=0$, $x=L_x$ and $y=0$, $y=L_y$, on the middle plane, whether it represents or not the reference plane Ω:

$$w^0(0,y)=0\ ;\ w^0(L_x,y)=0\ ;\ w^0(0,y)_{,xx}=0\ ;\ w^0(L_x,y)_{,xx}=0$$

$$w^0(x,0)=0\ ;\ w^0(x,L_y)=0\ ;\ w^0(x,0)_{,yy}=0\ ;\ w^0(x,L_y)_{,yy}=0 \tag{7}$$

L_x, L_y being the length of sides parallel to x, y axes, respectively. In the applications, plates in cylindrical bending are considered, whose boundary conditions are derived in a straightforward way from (7). Obviously, e.g. if (x, z) is assumed as the plane where bending takes place, the appropriate conditions are obtained assuming that variations in the y direction are nil.

At clamped edges, the following constraints are imposed at the middle-plane z^*, which as an example are reported in the case the extreme is at $x=0$:

$$u_\alpha(0,z^*) = w_\varsigma(0,z^*) = w_\alpha(0,z^*)_{,x} = 0 \tag{8}$$

In order to simulate that the previous conditions hold identically across the thickness, the following further boundary conditions are enforced:

$$u_\alpha(0,z)_{,z} = 0 \ ; \ u_\varsigma(0,z)_{,z} = 0 \ ; \ u_\varsigma(0,z)_{,xz} = 0 \tag{9}$$

In addition, the mechanical boundary condition:

$$\int_{-h/2}^{h/2} \sigma_{xz}(0,z)dz = T \tag{10}$$

is imposed in order to ensure that the transverse shear stress resultant force per unit of width equals the counterpart constraint force T.

The additional support condition $w^0(L,z_l) = 0$ holds at $x=L$ on the lower face z_l at the supported extreme of the propped cantilever beam considered in the numerical applications. In this case, condition (10) is reformulated as: $\int_{-h/2}^{h/2} \sigma_{xz}(L,z)dz = T_L$. Note that the mechanical boundary conditions defined above are enforced using Lagrange multipliers method.

After expressing $\Re^i(x,y)$ as defined above for the single case, the candidate solution (6) of (1) issubstituted into the expression of TPE, which is constructed using the relations, provided by the symbolic that comes from the enforcement of (2) to (5). Loading distributions considered in the numerical applications are represented by the symbolic calculus tool used to construct the present structural model as analytical continuous or discontinuous functions, whose energy contribution is computed exactly.

III. NUMERICAL ASSESSMENTS AND DISCUSSION

Elasto-static benchmarks whose lay-ups, loading and boundary conditions enhance layerwise effects are considered for assessing accuracy and efficiency of the present 3-D approximate solution methodology. They are identified here as cases a to f and can be distinguished in two groups based on their specific characteristics.

The first group consists of cases b and c, for which the exact solution is available and then is retaken as reference solution together with one by 3-D FEA [24]. In other cases, only 3-D FEA is the reference solution. Moreover, results by laminated plate theories are reported, including those of accurate 3-D zig-zag theories such as ZZA and ZZA * [19-21].

Note that 3-D FEA [24] results are obtained using mixed solid finite elements [24] having the three elastic displacements and the three out-of-plane stress components as degrees of freedom are used, which respect the continuity of the above mentioned stresses at layer interfaces, how it is required to be, with no need for post processing, whose accuracy has been amply demonstrated by case applications even with singularities in the field.

These cases are considered for the purpose of assessing the accuracy of the approximate solution 3-D methodology proposed in this paper, thus avoiding that errors related to the approximations introduced can render the interpretation doubtful, as would happen with any approximate solution method whenever it is used as a comparison solution. As a consequence, comparisons between 3-D FEA and exact solution enable to further test accuracy of 3-D FEA [24], in order to avoid that the conclusions drawnfor cases a and d to f are not invalidated by doubts concerning calculation errors.

3.1 Case A

This case concerns a propped cantilever sandwich beam under a uniform transverse loading applied on its upper face, i.e. whose edges are clamped at x=0 and supported at x=Lx at the bottom layer, having a length-to-thickness ratio of 14.268. Nevertheless this case is not extremely thick, as instead usually considered when testing theories in order to boost 3-D effects, strong layerwise effects occur because of its material properties and loading and boundary conditions, as evidenced also by the results of theories HRZZ, HRZZ4, MHWZZA, MHWZZA4, MHR and MHR4 reported in [21], in comparison to the higher order theory ZZA [19], which are all together reported in this paper for demonstration purposes.

HRZZ and HRZZ4 are two mixed HR physically-based theories whose in-plane displacement is the same of ZZA, while transverse one is uniform and fourth-order polynomial respectively (stresses apart from local equilibrium equations). MHR

and MHR4 are two kinematic-based theories that include Murakami's zig-zag function into in-plane displacement, while transverse one is fourth-order and piecewise polynomial respectively. Instead, MHWZZA and MHWZZA4 has the same displacement field of MHR (MHWZZA4 has also the same transverse displacement of ZZA), while strains and stresses are retaken from HWZZ. The latter theory is a mixed HW (strains and stresses assumed independently from kinematics) physically-based adaptive zig-zag theory, whose coefficients, differently to previous theories, are redefined for each layer across the thickness by imposing the full set of physical constraints (2) to (5).

As shown by Figure 2, a large dispersion of results is highlighted for in-plane and transverse displacements, the cause being the still too poor kinematics of HRZZ to MHR compared to ZZA, the latter having a redefinition of coefficients similar to that of the present theory, from which it differs only in the fact it still adopts a model across the thickness, which although it is very general it is still predefined a priori. Because of their shortcomings, theories HRZZ to MHR incorrectly predict transverse shear and normal through-thickness stress fields in the most critical region considered, as compared to 3-D FEA results (whose degree of accuracy will be highlighted below). On the contrary ZZA and the present approximate 3-D solution show results in agreement with each other and with 3-D FEA for all quantities and everywhere.

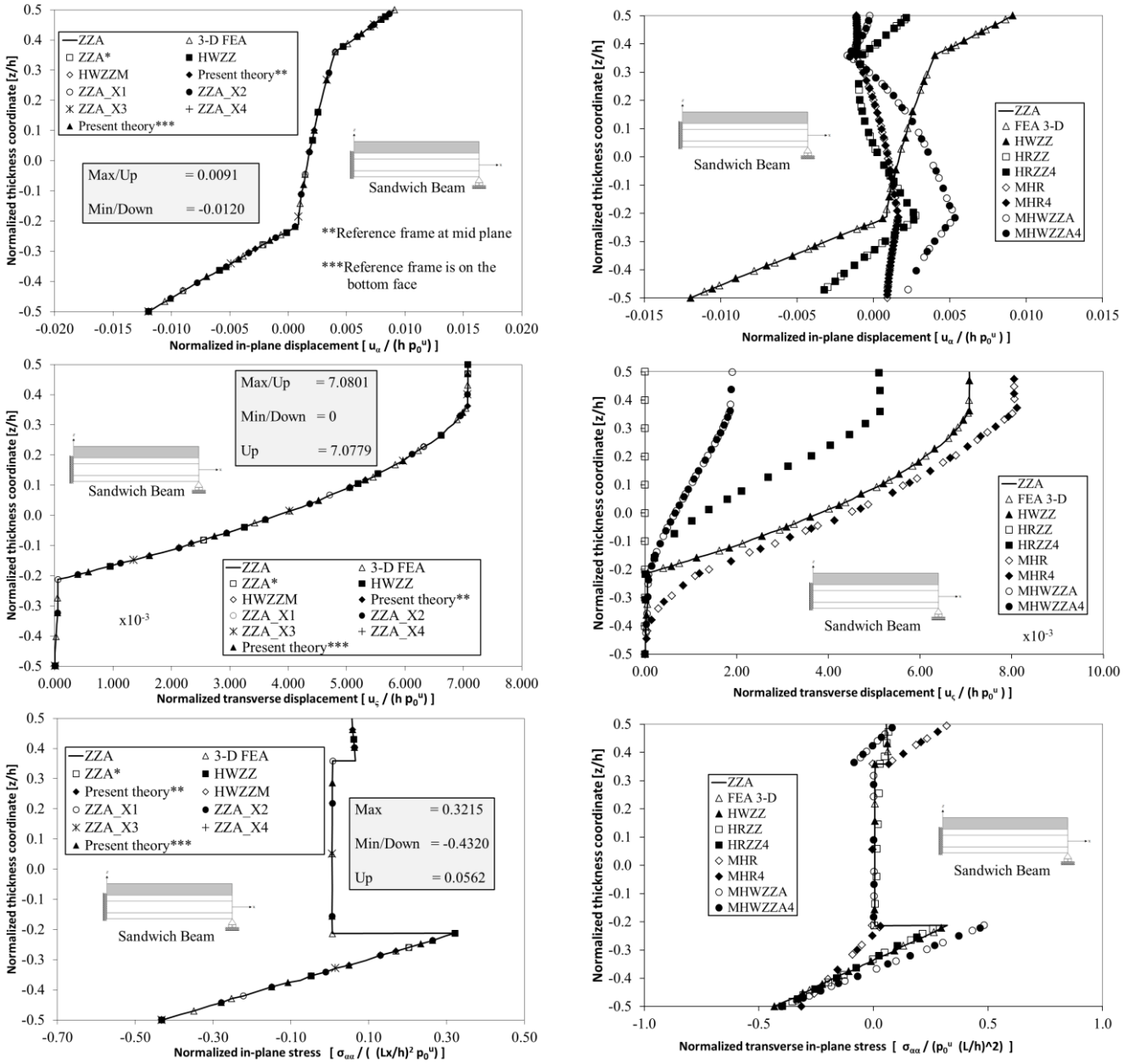

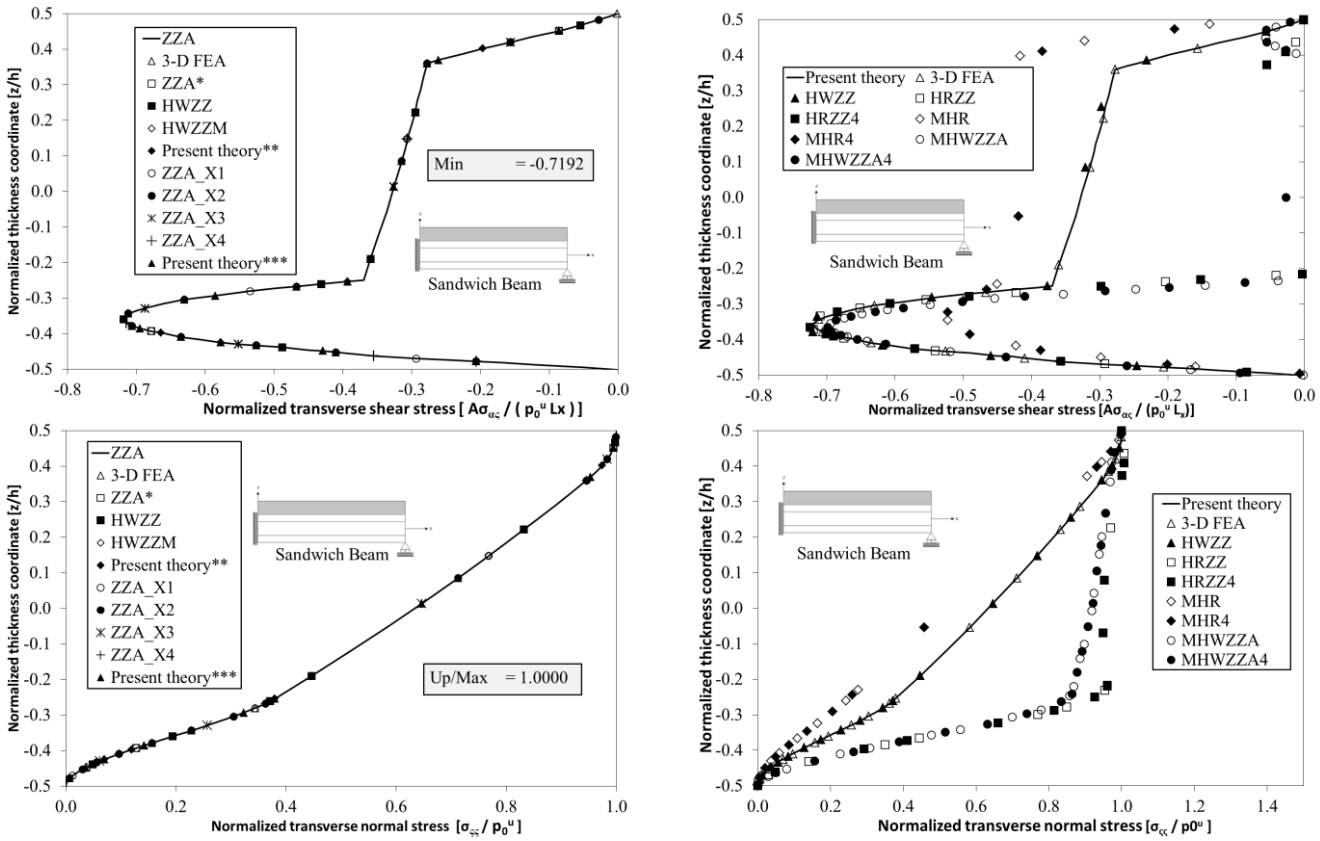

FIGURE 2: Case a: Normalized displacements and stresses, propped cantilever sandwich beam under a uniform loading.

The figure also shows the values assumed by the present theory at the top (Up) and bottom (Down) of the laminate and the maximum (Max) and minimum (Min) values across the thickness.

In addition to demonstrating the accuracy and efficiency (see Table 4 giving the processing time) of the present approximate 3-D solution search procedure, the results of Figure 2 also offer the possibility to comment on the requirements that the theories should have to accurately capture all the 3-D effects that are relevant.

TABLE 4

COMPUTATIONAL EFFORT [S] FOR THE EXAMINED CASES AND THEORIES.

	Theory	Case a	b	c	d	e	f
	FSDT	4.0338	2.2857	4.0928	1.8971	7.2570	4.0293
	Present theory	13.1075	4.1127	8.6521	4.2235	16.2312	9.0803
	ZZA_X1	11.9180	3.7531	7.9473	3.8206	14.7913	8.1602
(arbitrary representation)	ZZA_X2	12.2758	3.8442	8.0691	3.9522	15.1387	8.4179
	ZZA_X3	12.3912	3.8573	8.2443	4.0019	15.4243	8.5103
	ZZA_X4	12.5271	3.8553	8.1855	3.9869	15.3804	8.4476
Mixed HW	HWZZ	12.7078	4.4355	6.4151	5.1020	15.3278	6.6966
(Murakami's zigzag u^3,v^3,w^4)	HWZZM	12.7083	3.9657	8.4218	4.0728	15.7581	8.7583
(adaptive)	ZZA	15.7617	4.9446	10.4055	5.0946	19.4522	10.8600
(no zig-zag functions u^3,v^3,w^4)	ZZA*	11.8971	3.6656	7.7602	3.7789	14.6491	8.1071

Computer with quad-core CPU@2.60GHz, 64-bit OS and 8.00 GB RAM. Processing time is defined apart from the symbolic procedure used to create the model (which takes less than 10 seconds).

Nevertheless Murakami's rule is respected; theories MHR, MHR4, MHWZZA and MHWZZA4 using Murakami's zig-zag function provide very inaccurate results which demonstrate that physically-based theories HRZZ, HRZZ4 and ZZA, whose zig-zag amplitudes are recalculated at layer interfaces by enforcing stress compatibility conditions (2) like for the present approximate solution approach, are ones suitable for analysis. Findings of Figure 2 also show that an accurate description of transverse displacement is mandatory for the present case a, since HRZZ and HRZZ4 (that assume a uniform and a polynomial representation for u_ς, while in-plane displacement is piecewise polynomial) cannot reach the same precision of the present theory, ZZA, HWZZ, ZZA*, HWZZM [20], ZZA_X1 to ZZA_X4 [26], which have coefficients that are redefined across the thickness as common feature. It should be noticed that two different reference frames are assumed for the present theories (the first one is assumed at the middle plane of plate, while the second one is assumed coincident with the bottom face of plate). Particularly, HWZZM is a mixed physically-based HW theory that includes Murakami's zig-zag function and a second order zig-zag one are used instead of ZZA ones; strains and stresses are assumed apart like in HWZZ. Zig-zag functions are omitted in ZZA* while different representations (than power series of z) of transverse variation from point to point for each displacement are assumed for ZZA_X1 to ZZA_X4. Because of the results of these latter cited theories ZZA to ZZA_X4 and ones by the present 3-D approximate solution procedure are indistinguishable from each other, it is demonstrated that the choice of zig-zag and representation functions is immaterial, if coefficients are redefined for each layer so that the full set of physical constraints (2) to (5) is imposed. Because, as shown in [21] in a broader way from the point of view of the cases examined, all theories that only partially satisfy (2) to (5) give results that depends on the choices made for zig-zag and representation functions and whose accuracy degree results strongly case-sensitive, none of them is worthy of being used for comparisons with the present 3-D solution, nor for use in the analyses. Table 4shows the processing time of the present approximate 3-D approach and those of theories ZZA, ZZA*, HWZZ, HWZZM, ZZA_X1 to ZZA_X4. The computational effort of other theories is not reported, but they are similar to those of previous ones, which are still comparable to those of ESL [21]. Because of HRZZ, HRZZ4, MHWZZA, MHWZZA4, MHR and MHR4 are less accurate than the present theory, ZZA, ZZA*, HWZZ, HWZZM, ZZA_X1 to ZZA_X4, they will not be reported for the following cases.

Apart from the comments on the behavior of the various theories, on the basis of their approximations, it is evident that the proposed approach is accurate and therefore can be used profitably as a reference solution when the exact one is not available.

3.2 Cases B and C

Case b is a [0/90/0] multilayered simply-supported beam under a sinusoidal loading, whose constituent layers are made of the same material. This case is considered, although it is not particularly severe from the standpoint of layerwise effects, given the existence of the exact solution that lends itself suitable both to assess the accuracy of this procedure, and simultaneously that of 3-D FEA.

Results provided by the present solution methodology those by 3-D FEA and ones by ZZA, ZZA*, HWZZ, HWZZM, ZZA_X1 to ZZA_X4 are compared to the exact solution by Pagano retaken from [17], as shown in Figure 3. It is shown that all theories considered in this figure are able to accurately predict displacements and stresses, their results being very close to exact solutions. Since the theories considered are based on different assumptions as regards the functions that characterize the representation across the thickness as well as zig-zag functions, the uniformity of the results shows that also in this case it can be argued that the choice of zig-zag function and of the representation form can be freely chosen, with the former that even be omitted if coefficient of theories are recalculated for each layer through the enforcement of (2) to (5). Anyway, the results show that the present 3-D approximate solution approach and 3-D FEA provide very accurate results compared to exact solution, therefore they lend themselves to be used as comparison solutions in the cases in which arbitrary lay-ups, loading and boundary conditions are considered. Like the previous cases, Table 4 shows the processing time of all theories that are always comparable to those of ESL.

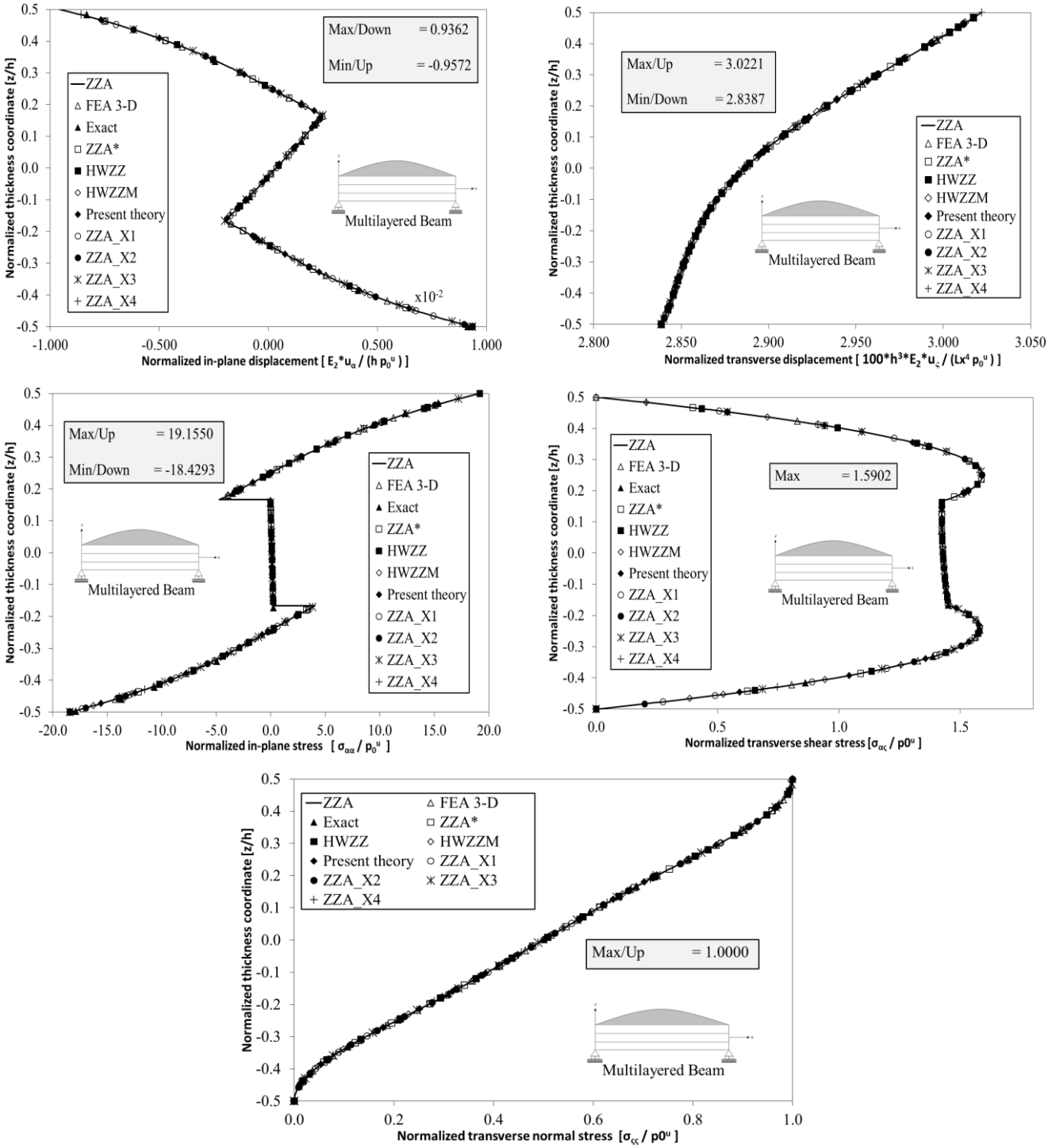

FIGURE 3: Case b: Normalized displacements and stresses, simply-supported laminated beam under a sinusoidal loading.

Regarding case c (Figure 4), it is a simply-supported rectangular sandwich plate, previously studied by Brischetto et al. [27]. Faces have different thickness and are made of different materials and results provided by ZZA, ZZA*, HWZZ, HWZZM, ZZA_X1 to ZZA_X4 and 3-D FEA are compared to exact ones. Indistinguishable results are obtained by previously cited theories, so, the same considerations of cases a and b still apply.

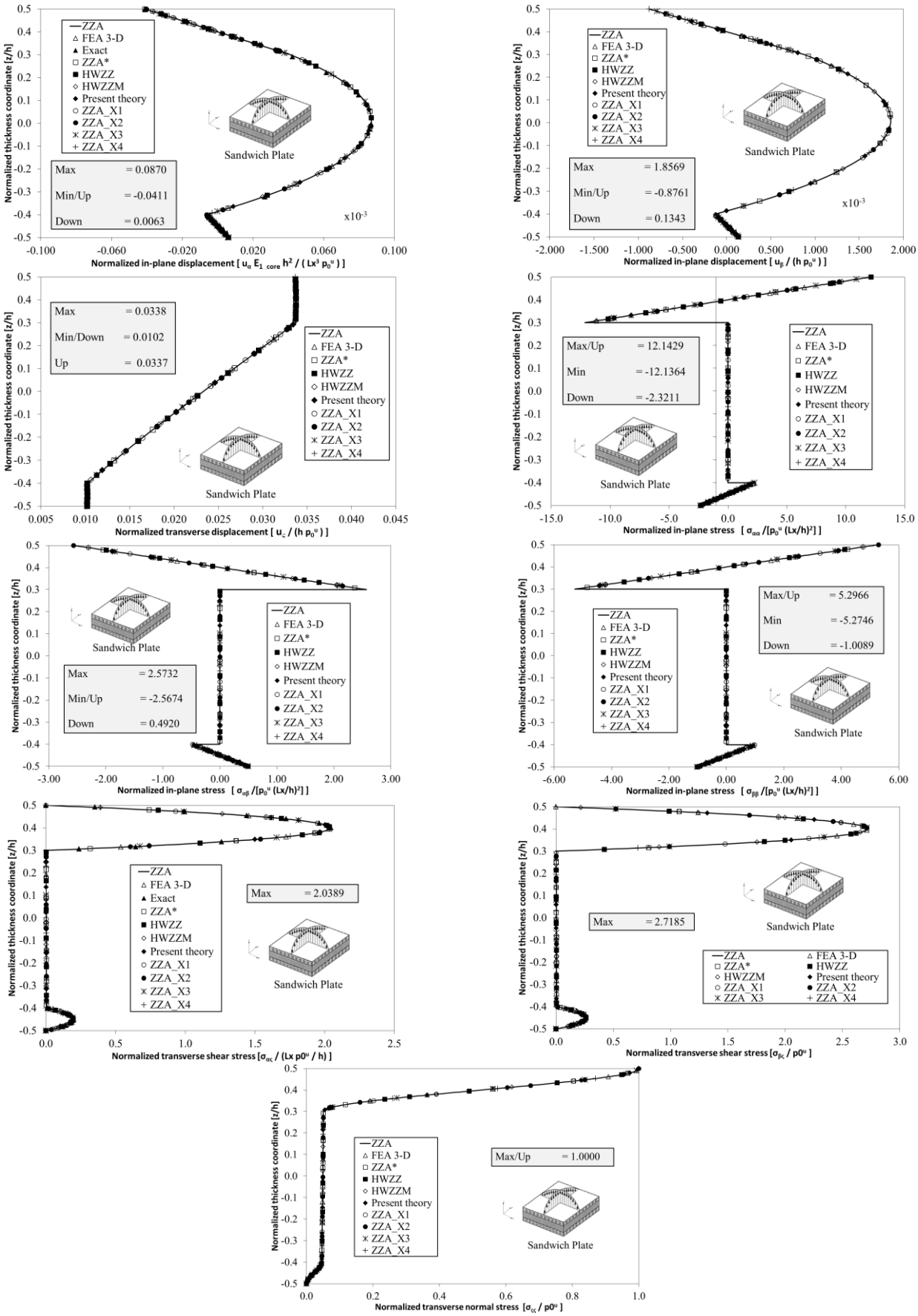

FIGURE 4: Case c: Normalized displacements and stresses, simply-supported rectangular sandwich plate under a bi-sinusoidal loading.

Nevertheless results of cases b and c have demonstrated the high-accuracy of the present solution procedure, further benchmarks with localized loading or damaged layers have to be considered to state with certainty that it and 3-D FEA as well can be used as comparison solutions in cases whenever the exact solution is not available.

Also in these cases, the present approximate 3-D solution approach appears accurate and then valuable as a reference solution.

3.3 Cases D, E and F

In order to comply with the need expressed in the previous sentence at the end of the previous section, three kinds of simply supported beams and plates are considered, whose displacement and stress fields are difficult to capture because of their strong layerwise effects due to the types of loading considered, which do not admit exact solution despite the constraints are those less burdensome in terms of modeling.

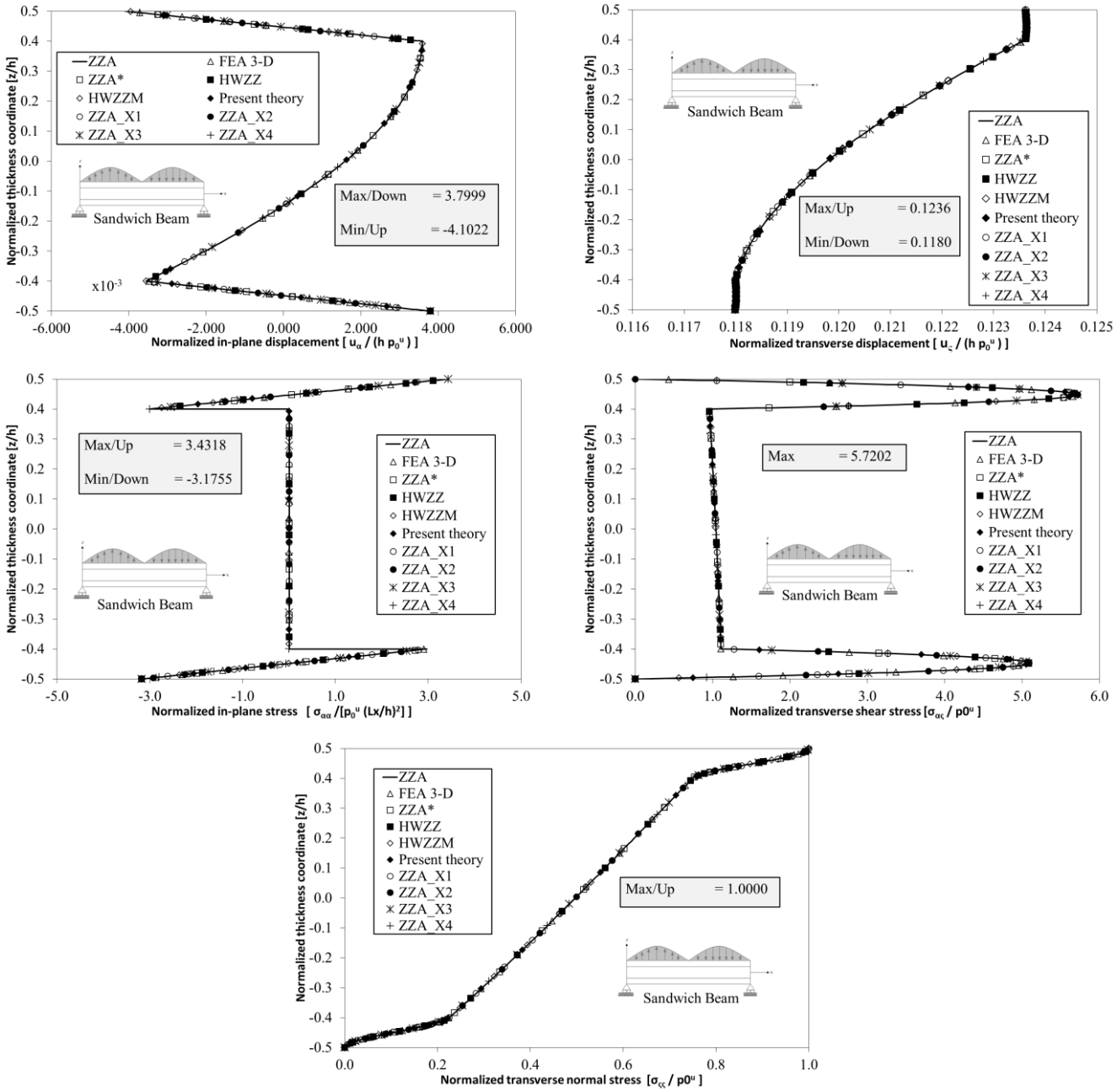

FIGURE 5: Case d: Normalized displacements and stresses, simply-supported sandwich beam under a sinusoidal loading (two half-waves).

Case d (Figure 5) is a simply-supported sandwich beam under a two half waves sinusoidal loading on the upper face, case e (Figure 6) is a simply-supported laminated beam under a uniform loading applied on the same face for $x \leq Lx/2$ and on the lower one for $x > Lx/2$ having an opposite sign. Case f (Figure 7) is a simply-supported sandwich rectangular plate (length-to-thickness and length-to-side ratios are 4 and 3 respectively), under a bi-sinusoidal loading and with the lower face damaged (elastic modulus E1111, E1122, E2222, E1212 of the first layer from below are reduced by a factor of 2·10-1). This latter case is considered because this condition can occur during the service life, for example as a result of impact damage. Anyway, all these cases represent severe tests for models and for this region they are chosen. They show an asymmetric behavior across the thickness, either because of their lay-ups, material properties or loading conditions.

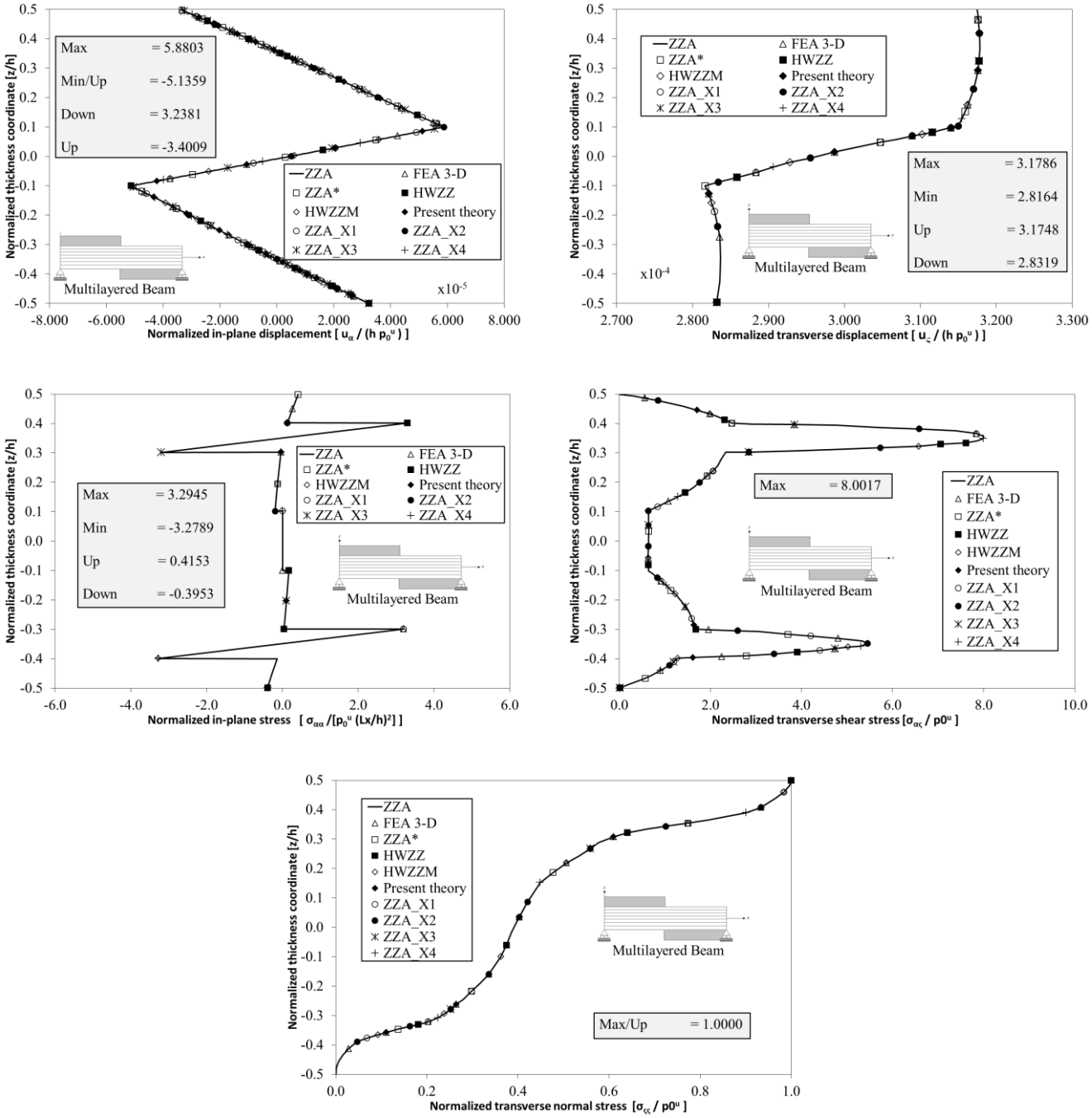

FIGURE 6: Case e: Normalized displacements and stresses, simply-supported laminated beam under localized step loading.

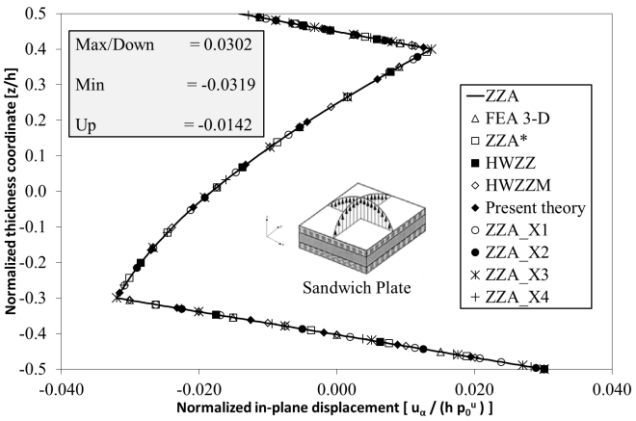
Max/Down = 0.0302
Min = -0.0319
Up = -0.0142
ZZA
FEA 3-D
ZZA*
HWZZ
HWZZM
Present theory
ZZA_X1
ZZA_X2
ZZA_X3
ZZA_X4
Sandwich Plate
Normalized thickness coordinate [z/h]
Normalized in-plane displacement [u_α / (h p_0^u)]

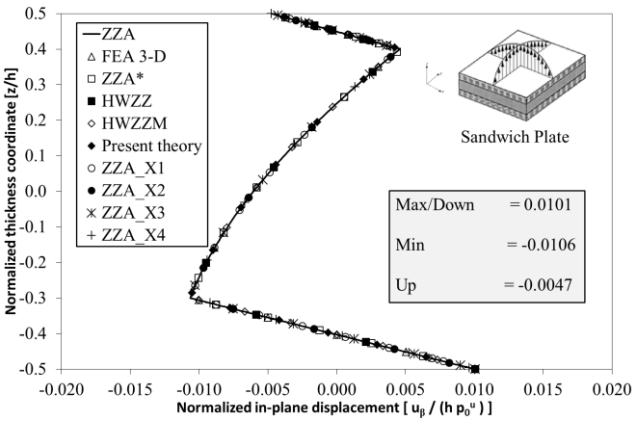
ZZA
FEA 3-D
ZZA*
HWZZ
HWZZM
Present theory
ZZA_X1
ZZA_X2
ZZA_X3
ZZA_X4
Sandwich Plate
Max/Down = 0.0101
Min = -0.0106
Up = -0.0047
Normalized thickness coordinate [z/h]
Normalized in-plane displacement [u_β / (h p_0^u)]

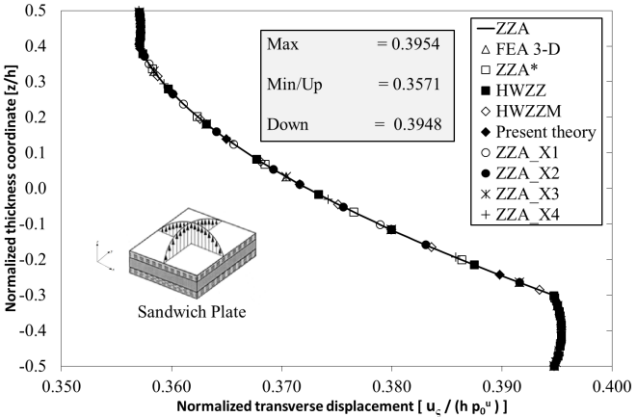
Max = 0.3954
Min/Up = 0.3571
Down = 0.3948
ZZA
FEA 3-D
ZZA*
HWZZ
HWZZM
Present theory
ZZA_X1
ZZA_X2
ZZA_X3
ZZA_X4
Sandwich Plate
Normalized thickness coordinate [z/h]
Normalized transverse displacement [u_z / (h p_0^u)]

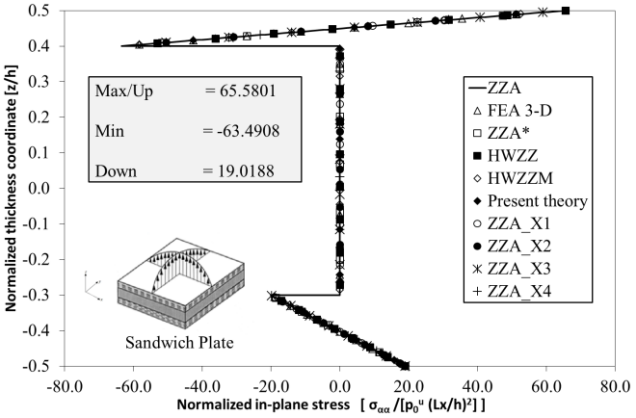
Max/Up = 65.5801
Min = -63.4908
Down = 19.0188
ZZA
FEA 3-D
ZZA*
HWZZ
HWZZM
Present theory
ZZA_X1
ZZA_X2
ZZA_X3
ZZA_X4
Sandwich Plate
Normalized thickness coordinate [z/h]
Normalized in-plane stress [$\sigma_{\alpha\alpha}$ /[p_0^u (Lx/h)²]]

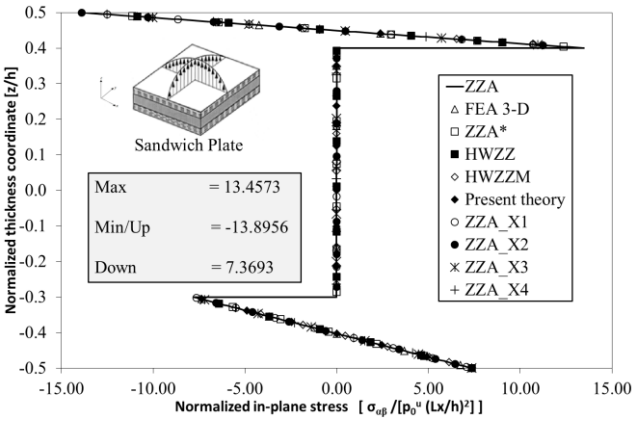
Max = 13.4573
Min/Up = -13.8956
Down = 7.3693
ZZA
FEA 3-D
ZZA*
HWZZ
HWZZM
Present theory
ZZA_X1
ZZA_X2
ZZA_X3
ZZA_X4
Sandwich Plate
Normalized thickness coordinate [z/h]
Normalized in-plane stress [$\sigma_{\alpha\beta}$ /[p_0^u (Lx/h)²]]

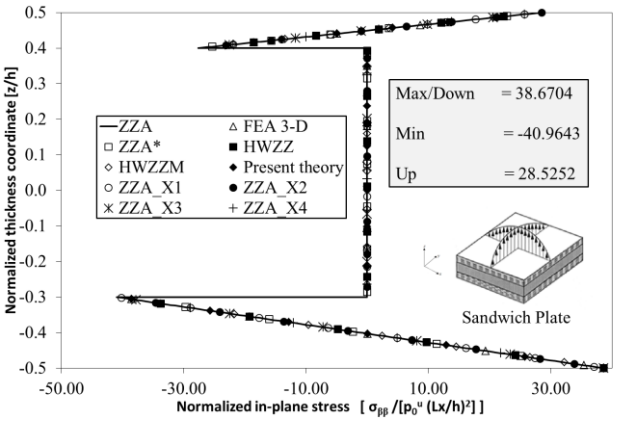
Max/Down = 38.6704
Min = -40.9643
Up = 28.5252
ZZA
FEA 3-D
ZZA*
HWZZ
HWZZM
Present theory
ZZA_X1
ZZA_X2
ZZA_X3
ZZA_X4
Sandwich Plate
Normalized thickness coordinate [z/h]
Normalized in-plane stress [$\sigma_{\beta\beta}$ /[p_0^u (Lx/h)²]]

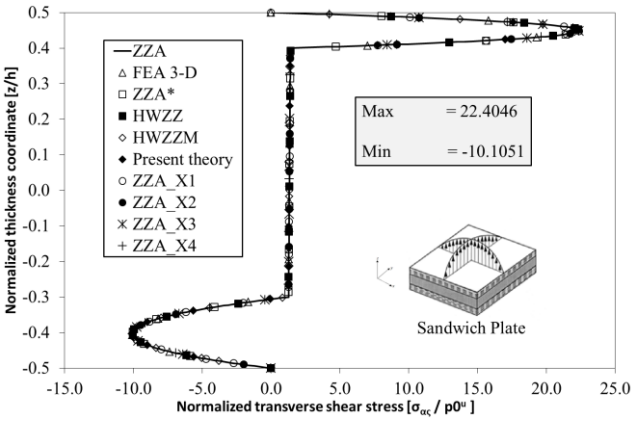
Max = 22.4046
Min = -10.1051
ZZA
FEA 3-D
ZZA*
HWZZ
HWZZM
Present theory
ZZA_X1
ZZA_X2
ZZA_X3
ZZA_X4
Sandwich Plate
Normalized thickness coordinate [z/h]
Normalized transverse shear stress [$\sigma_{\alpha\zeta}$ / p0^u]

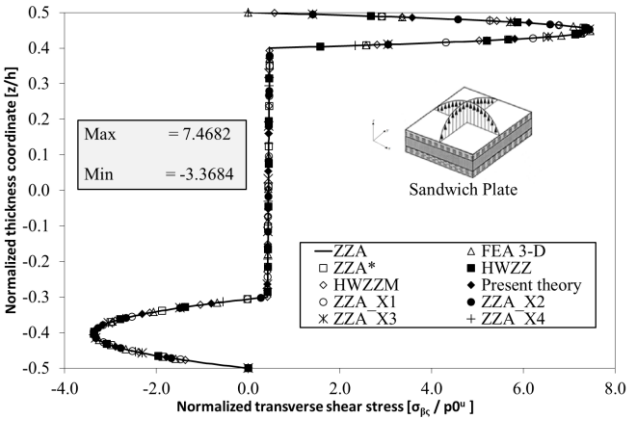
Max = 7.4682
Min = -3.3684
Sandwich Plate
ZZA
FEA 3-D
ZZA*
HWZZ
HWZZM
Present theory
ZZA_X1
ZZA_X2
ZZA_X3
ZZA_X4
Normalized thickness coordinate [z/h]
Normalized transverse shear stress [$\sigma_{\beta\zeta}$ / p0^u]

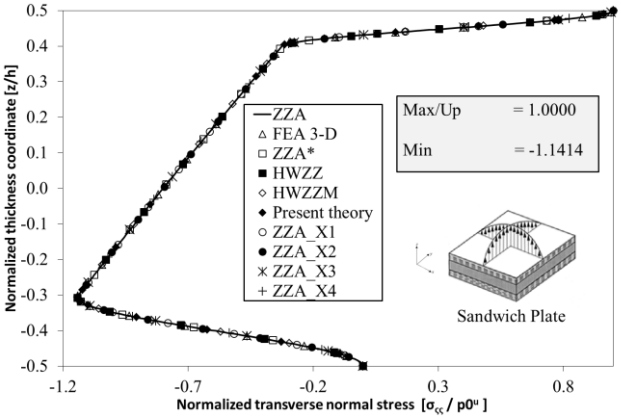

FIGURE 7: Case f: Normalized displacements and stresses, simply-supported rectangular sandwich plate under a bi-sinusoidal loading. The lower face is damaged by a factor of $2 \cdot 10^{-1}$.

The results by the present approximate 3-D solution approach and the ones by the theories already mentioned above, which recall its characteristics due to the fact that coefficients are redefined across the thickness, although they are based on different assumptions from each other, are compared to the results of 3-D FEA, as done previously.

For cases d and e, in-plane displacement and transverse shear stress are shown at x=0, while the other quantities (transverse displacement, in-plane and transverse normal stresses) are shown at x/Lx=0.25.

It can be seen that the present approximate solution approach and those of theories ZZA, ZZA*, HWZZ, HWZZM and ZZA_X1 to ZZA_X4, whose coefficients are redefined for each mathematical or physical layers through the enforcement of the full set of physical constraints (2) to (5) are equally accurate, their results being very close to those of 3-D FEA.

The results of other theories considered in [21], here not reported so as not to complicate the graphics too much, on the contrary show discrepancies that indicate their lower predictive capability, also in virtue of a partial satisfaction of constraints, which results in a strong dependence of the assumptions made concerning the type of representation and the zigzag functions chosen. Table 4 shows once again and for the present cases that the processing time of all theories is still always comparable to that of ESL although to their accuracy it is much higher, therefore in fact attesting to their efficiency. Again, the present approximate 3-Dsolution approach proves to be efficient, accurate and suitable as a reference solution.

IV. CONCLUDING REMARKS

A 3-D approximate solution procedure has been proposed in this paper which avoids assuming any restrictive hypotheses across the thickness about through-thickness kinematics, strain and stress fields, like on the contrary usually done for developing laminated plate theories so to overcome algebraic difficulties.

A general representation of variables is assumed, which is based on a fixed number of unknowns irrespective for the number of constituent layers, whose intended aim is to capture all the salient three-dimensional effects with a low computational cost, so to provide a quick and accurate tool that provides a reference results for cases where exact solutions cannot be found with the known techniques, due to the considered lay-up, loading and boundary conditions.

It comes to constitute a generalization of zig-zag theories [19-21], which likewise uses a fixed number of d.o.f. irrespective of the number of layers, for the ideas on the basis of which it is developed. The fundamental aspect to underline is the lack of zig-zag layerwise functions, as the coefficients of the displacement field play themselves the role of layerwise functions being redefined across the thickness through the enforcement of physical constraints related to out-of-plane compatibility of stress components, displacements and fulfillment of stress-boundary conditions.

The characteristic feature that enables the development of such a general physically-based theory is that all constraints are satisfied in exact form through use of a symbolic calculus tool that provides once and for all expressions deriving from the enforcement of constraints. An analytical solution is searched as a truncated expansion series of trial functions and unknown amplitudes using Rayleigh-Ritz and Lagrange multipliers methods.

To assess its accuracy, a number of challenging benchmarks with strong layerwise effects have been considered, along with applications with less demanding characteristics from the standpoint of modeling, for which exact solutions are available.

The results of all these applications show that invariably the present approximate 3-D solution turns out to be accurate and of low cost, as shown by the comparison with the exact results when available and the results of 3-D FEA and by recent laminated plate theories by the authors, which although presenting similar characteristics as the lack of explicit zigzag functions and the imposition of strict constraints across the thickness are however based on a priori assumptions

REFERENCES

[1] E. Carrera, "Developments, ideas, and evaluations based upon Reissner's mixed variational theorem in the modeling of multilayered plates and shells," Appl. Mech. Rev., 2001, vol. 54, pp. 301-329.

[2] E. Carrera, "Historical review of zig-zag theories for multilayered plates and shells," Appl. Mech. Rev., 2003, vol. 56, pp. 1-22.

[3] E. Carrera, "On the use of the Murakami's zig-zag function in the modeling of layered plates and shells," Compos. Struct., 2004, vol. 82, pp. 541–554.

[4] E. Carrera, and A. Ciuffreda, "Bending of composites and sandwich plates subjected to localized lateral loadings: a comparison of various theories," Composite Structures, 2005, vol. 68, pp. 185–202.

[5] V.V. Vasilive, and S.A. Lur'e, "On refined theories of beams, plates and shells," J. Compos. Mat., 1992, vol. 26, pp. 422–430.

[6] J.N. Reddy, and D.H. Robbins, "Theories and computational models for composite laminates." Appl. Mech. Rev., 1994, vol. 47, pp. 147–165.

[7] S.A. Lur'e, and N.P. Shumova, "Kinematic models of refined theories concerning composite beams plates and shells," Int. J. Appl. Mech., 1996, vol. 32, pp. 422-430.

[8] A.K. Noor, S.W. Burton, and C.W. Bert, "Computational model for sandwich panels and shells," Appl. Mech. Rev., 1996, vol. 49, pp. 155–199.

[9] H. Altenbach, "Theories for laminated and sandwich plates. A review," Int. J. Appl. Mech., 1998, vol. 34, pp. 243-252.

[10] R. Khandan, S. Noroozi, P. Sewell, and J. Vinney, "The development of laminated composite plate theories: a review," J. Mater. Sci., 2012, vol. 47, pp. 5901-5910.

[11] S. Kapuria, and J.K. Nath, "On the accuracy of recent global–local theories for bending and vibration of laminated plates," Compos. Struct., 2013, vol. 95, pp. 163–172.

[12] J.N. Reddy, "Mechanics of laminated composite plates and shells: Theory and analysis.(2nd ed)," 2003, Boca Raton: CRC Press.

[13] S. Brischetto, "Exact three-dimensional static analysis of single- and multi-layered plates and shells," Composites Part B Engineering, 2017, vol. 119, pp. 230-252.

[14] Y. Yang, A. Pagani, and E. Carrera, "Exact solutions for free vibration analysis of laminated, box and sandwich beams by refined layer-wise theory," Composite Structures, 2017,vo. 175, pp. 28–45.

[15] U. Icardi, "Higher-order zig-zag model for analysis of thick composite beams with inclusion of transverse normal stress and sublaminates approximations," Compos. Part B., 2001, vol. 32, pp. 343-354.

[16] J.G Ren, "Exact solutions for laminated cylindrical shells in cylindrical bending," Composites Science and Technology, 1987, vol. 29, pp. 169-187.

[17] N.J. Pagano, "Exact solutions for composites laminates in cylindrical bending," J of Composite Materials, 1967, vol. 3, pp. 398-411.

[18] N.J. Pagano,"Exact Solutions for Rectangular Bidirectional Composites and Sandwich Plates," J of Composite Materials, 1970, vol. 4, pp. 20-34.

[19] U. Icardi, and F. Sola, "Development of an efficient zig-zag model with variable representation of displacements across the thickness," J. of Eng. Mech., 2014, vol. 140, pp. 531-541.

[20] U. Icardi, and A. Urraci, "Free and forced vibration of laminated and sandwich plates by zig-zag theories differently accounting for transverse shear and normal deformability."Aerosp. MDPI., 2018, vol. 5, pp. 108.

[21] U. Icardi., and A. Urraci,"Novel HW mixed zig-zag theory accounting for transverse normal deformability and lower-order counterparts assessed by old and new elastostatic benchmarks," Aer. Sci. & Tech., 2018, vol. 80, pp. 541-571.

[22] J.N. Reddy, and W.C. Chao, "A comparison of closed-form and finite element solutions of thick laminated anisotropic rectangular plates," Nuclear Engineering and Design, 1981, vol. 64, pp. 153-167.

[23] A.S.Yakimov, "Analytical Solution Methods for Boundary Value Problems. 1st Edition," 2016,Academic Press

[24] U. Icardi, and A. Atzori, "A. Simple, efficient mixed solid element for accurate analysis of local effects in laminated and sandwich composites," Advances in Eng. Software, 2004, vol. 35, pp. 843-859.

[25] S.S.Vel, and R.C. Batra, "Analytical solution for rectangular thick plates subjected to arbitrary boundary conditions,"1999, vol. 37, pp. 1464 - 1473.

[26] A.Urraci, and U. Icardi,"Zig-zag theories differently accounting for layerwise effects of multilayered composites," International Journal of Engineering Research & Science, 2019, vol. 5, pp. 21-42.

[27] S. Brischetto, E. Carrera, and L. Demasi, "Improved response of asymmetrically laminated sandwich plates by using zig-zag functions," J. Sandw. Struct. Mater., 2009, vol. 11, pp 257–267.

AD Publications
Sector-3, MP Nagar, Bikaner,
Rajasthan, India
www.adpublications.org, info@adpublications.org